NUREG/CR 0943
NRL Memorandum Report 4064

Structural Integrity of Water Reactor Pressure Boundary Components

Quarterly Progress Report, April–June 1979

F. J. Loss, Editor

Thermostructural Materials Branch
Material Science and Technology Division

September 28, 1979

Prepared for U.S. Nuclear Regulatory Commission

NAVAL RESEARCH LABORATORY
Washington, D.C.

NOTICE

Available from
National Technical Information Service
Springfield, Virginia 22161

SECURITY CLASSIFICATION OF THIS PAGE (When Data Entered)

REPORT DOCUMENTATION PAGE

READ INSTRUCTIONS BEFORE COMPLETING FORM

1. REPORT NUMBER NUREG/CR 0943 NRL Memorandum Report 4064	2. GOVT ACCESSION NO. / 3. RECIPIENT'S CATALOG NUMBER
4. TITLE (and Subtitle) STRUCTURAL INTEGRITY OF WATER REACTOR PRESSURE BOUNDARY COMPONENTS – QUARTERLY PROGRESS REPORT, APRIL–JUNE 1979	5. TYPE OF REPORT & PERIOD COVERED Interim report on a continuing NRL problem. 6. PERFORMING ORG. REPORT NUMBER
7. AUTHOR(s) F. J. Loss, Editor	8. CONTRACT OR GRANT NUMBER(s) NRC-RES 79-103 NRC FIN B5528
9. PERFORMING ORGANIZATION NAME AND ADDRESS Naval Research Laboratory Washington, DC 20375	10. PROGRAM ELEMENT, PROJECT, TASK AREA & WORK UNIT NUMBERS NRL Problem M01-40
11. CONTROLLING OFFICE NAME AND ADDRESS U.S. Nuclear Regulatory Commission Office of Nuclear Regulatory Research Washington, DC 20555	12. REPORT DATE September 28, 1979 13. NUMBER OF PAGES 68
14. MONITORING AGENCY NAME & ADDRESS(if different from Controlling Office)	15. SECURITY CLASS. (of this report) UNCLASSIFIED 15a. DECLASSIFICATION/DOWNGRADING SCHEDULE

16. DISTRIBUTION STATEMENT (of this Report)

Approved for public release; distribution unlimited.

17. DISTRIBUTION STATEMENT (of the abstract entered in Block 20, if different from Repo

18. SUPPLEMENTARY NOTES

Prepared for the U.S. Nuclear Regulatory Commission, Office of Nuclear Regulatory Research, Reactor Safety Research Division under Interagency Agreement RES 79-103.
NRC Distribution Category R5 and AN

19. KEY WORDS (Continue on reverse side if necessary and identify by block number)

Nuclear pressure vessel steels	Radiation sensitivity
J-integr , R curve	Postirradiation recovery
Single specimen compliance test	A533-B submerged arc weld
Charpy-V test	Microstructure

20. ABSTRACT (Continue on reverse side if necessary and identify by block number)

This report describes research progress in a continuing program to characterize materials properties performance with respect to structural integrity of light water reactor pressure boundary components. Progress for this reporting period is summarized in the following areas: (a) post-irradiation fracture toughness of IAEA coordinated program steels, (b) Charpy V-notch ductility trends of submerged arc weld deposit with cyclic postirradiation annealing and reirradiation treatments, (c) J-R curve characterization of irradiated submerged arc weld deposits, and (d) evaluation of critical factors in cyclic crack growth rate studies in a pressurized water reactor environment.

DD FORM 1 JAN 73 1473 EDITION OF 1 NOV 65 IS OBSOLETE
S/N 0102-014-6601

SECURITY CLASSIFICATION OF THIS PAGE (When Data Entered)

CONTENTS

STRUCTURAL INTEGRITY OF WATER REACTOR PRESSURE BOUNDARY COMPONENTS

QUARTERLY PROGRESS REPORT, APRIL-JUNE 1979

SUMMARY

I. RADIATION SENSITIVITY AND POSTIRRADIATION PROPERTIES RECOVERY

A. Evaluation and Comparison of IAEA Coordinated Program Steels and Welds with 288°C Irradiation

Four steel materials supplied by Japan to the IAEA Program on "Analysis of the Behavior of Advanced Reactor Pressure Vessel Steels Under Neutron Irradiation," have been compared after 288°C irradiation against the IAEA reference steel plate (HSST Plate 03). Notch ductility comparisons indicate the Japanese materials to be somewhat more resistant to radiation-induced embrittlement than the reference material. The observed difference is believed due to a copper content difference (.01%Cu, max, Japanese-produced materials vs .12%Cu, IAEA reference plate).

B. IAR Program Investigation of Charpy-V Notch Ductility Trends with Cyclic Postirradiation Annealing and Reirradiation Treatments

The notch ductility behavior of two submerged arc weld deposits with irradiation to $\sim 1.2 \times 10^{19}$ n/cm^2 >1 MeV followed by two full cycles of 399°C (750°F)-168 hr annealing and 288°C (550°F) reirradiation for $\sim 0.7 \times 10^{19}$ n/cm^2 has been determined. The total fluence received was $\sim 2.6 \times 10^{19}$ n/cm^2. The results demonstrate that the buildup of detrimental radiation effects can be reduced significantly by intermediate 399°C annealing and that the benefits can be retained through two cycles of reirradiation. The results also confirm an earlier observation with one cycle of reirradiation where the rate of reembrittlement of annealed material was found to be higher than that of non-annealed material for the same increment of additional fluence.

Note: Manuscript submitted July 23, 1979.

II. FRACTURE MECHANICS INVESTIGATIONS

A. J-R Curve Characterization of Irradiated Submerged Arc Weld Deposit

Upper shelf J-R curve trends of an irradiated A533-B submerged-arc weld metal having a high impurity copper level have been characterized as a function of cyclic postirradiation annealing and reirradiation. Irradiation to a fluence of 1.2×10^{19} n/cm^2, >1 MeV reduced the upper shelf J_{Ic} level by one-half, to a value of 65 kJ/m^2 (373 lb/in.) or an equivalent K_{Jc} value of 119 MPa$\sqrt{m}$ (108 ksi$\sqrt{in.}$). The tearing modulus was reduced to a level of 30 which reflects approximately one-third of its unirradiated value. After one and two cycles of reirradiation, coupled with intermediate anneals, the toughness did not drop below the level of the original irradiation condition even though the total fluence was doubled. These results are consistent with the behavior defined by C_v upper shelf energy.

J-R curve trends were established with IT-CT specimens having 20 percent side grooves and using the single specimen compliance technique. Due to the nonlinear behavior of the R curve, an alternative definition of J_{Ic} is proposed in place of that given by the ASTM proposed multispecimen standard. An apparent new phenomenon of specimen hardening prior to cleavage failure was also uncovered.

III. FATIGUE CRACK PROPAGATION IN LWR MATERIALS

A. Evaluation of Critical Factors in Cyclic Crack Growth Rate Studies

The objectives of the preliminary matrix test plan have been met and the testing of the main matrix has begun. The basic conclusions drawn from these test results are: (a) combinations of long ramp times ($\geq$1 min) and low temperatures (93°C) result in growth rates which reside a factor of three to five above the ASME Section XI air default line, and (b) combinations of long ramp times and high temperatures (288°C) produce data which reside essentially on the air default line. The presence of a hold time, coupled with a long ramp, does not increase crack growth rates at either the high or low temperature. The influence of hold times for shorter ramp times will be investigated.

A hydrogen embrittlement model has been proposed to assist the explanation of these results. The hydrogen is produced by hydrolysis at the crack tip during any appreciable ramp time. The slower diffusion rate at low temperature results in accumulation of the hydrogen in the plastic enclave at the crack tip and results in hydrogen assisted crack growth with rates of three to five times faster than growth in non-hydrogen producing environments. At high temperature, the faster diffusion rates, possibly coupled with passivation of the crack tip by an oxide layer results in hydrogen transport through and beyond the plastic zone, and crack growth rates are depressed back to the levels of growth rates in air.

B. Fractographic and Microstructural Investigation of Fatigue Specimens of A302 Grade B Steel

Microstructural and fractographic studies have been performed on Type A302-B ferritic steel to characterize the failure processes and establish correlations with fatigue propagation data. Failed specimens were examined by scanning electron microscopy (SEM) and by energy dispersive x-ray microanalysis. SEM examinations of the fracture surfaces of specimens cut in the T-L direction revealed presence of inclusion bands above an observed ΔK threshold value. Subsequent x-ray image scans and corresponding energy spectra showed that the bands were manganese-sulfide inclusions. The inclusion bands resulted in increased crack growth rate in these specimens compared to the specimens cut in the L-T direction. The ΔK threshold value necessary to activate the inclusion bands is believed to be a measure of the cohesive strength between the inclusions and the material matrix.

STRUCTURAL INTEGRITY OF WATER REACTOR PRESURE BOUNDARY COMPONENTS

QUARTERLY PROGRESS REPORT, APRIL-JUNE 1979

RESEARCH PROGRESS

I. RADIATION SENSITIVITY AND POSTIRRADIATION PROPERTIES RECOVERY

A. Evaluation and Comparison of IAEA Coordinated Program Steels and Welds with 288°C Irradiation

J. R. Hawthorne

Background

The International Working Group on Reliability of Reactor Pressure Components (IWG-RRPC), sponsored by the International Atomic Energy Agency (IAEA), is conducting a coordinated study of the radiation embrittlement behavior of pressure vessel steels. The research program, formally identified as "Analysis of the Behavior of Advanced Reactor Pressure Vessel Steels Under Neutron Irradiation," was approved by the IAEA Director General in December 1976 [1]. A main goal is to undertake a cooperative study of the radiation embrittlement behavior of improved steels produced in various countries. The stated purpose is to "demonstrate that careful specification of reactor steels can eliminate the problem of potential failure including that caused by neutron irradiation and to demonstrate whether or not knowledge has advanced to the point where steel manufacture and welding technology can routinely produce steel reactor pressure vessels of high radiation resistance" [1].

Materials for the investigation (plate, forging, weld), representing current production practices are being supplied to the program by the Federal Republic of Germany, France and Japan. A United States-produced A533-B steel plate (HSST Plate 03) is being used as a reference material in a role similar to that played by the ASTM A302-B steel reference plate [2] in reactor vessel surveillance. Material irradiations are being carried out at 290°C $\pm$10°C. The target fluence range for the study is 1 to 3 x 10^{19} n/cm^2 >1 MeV.

The Naval Research Laboratory (NRL) is a participant in the IWG-RRPC study under IAEA Research Agreement No. 1661/CF. Particular interests of the NRL investigations include determinations of the irradiation characteristics of the coordinated program materials, the relative radiation resistance of USA versus

non-USA steel production, and the correlation of Charpy-V notch ductility, fracture toughness and strength changes with irradiation. Projected results will be of significant value to NRC Regulatory Guide 1.99 [3] for foreign steel evaluations and to current reactor vessel construction codes.

Progress

Charpy-V (C_v) and fatigue precracked C_v (PCC_v) specimens of five coordinated program materials have been irradiated at 288°C to approximately 1.5×10^{19} n/cm^2 >1 MeV. Four of the materials were supplied by Japan and include two plates, one forging and one weld deposit. The fifth material is the IAEA reference plate. The irradiations were conducted in two experiments in the State University of New York at Buffalo, using its 2 MW pool reactor (UBR). The irradiation period was 630 hours for both experiments. Postirradiation C_v tests have been completed and are reported here; PCC_v testing is underway.

Table 1 identifies the materials by producer, chemistry and heat treatment. Tensile properties are given in Table 2. It will be noted that Plate LG was the parent plate for Weld JW 502. Pre- and postirradiation C_v results are given in Figs. 1 to 5 and are summarized in Table 3. Several observations are permitted by the data as follows:

1. The C_v 41J and C_v 68J transition temperatures for the Japan-produced materials are considerably lower than those of the IAEA reference plate for the unirradiated condition and for the irradiated condition.

2. The C_v 41J transition temperature elevations by irradiation for the Japan-produced materials were smaller than that for the IAEA reference plate (14 to 31°C versus 44°C). Of the former, the forging showed the greatest transition elevation with irradiation.

3. All of the materials exhibited high (≥135J) upper shelf energy levels before and after irradiation. For the most part, upper shelf reductions were less than 14J. The largest reductions (≥41J) were exhibited by the two Japan-produced plates. However, the preirradiation upper shelf levels of these plates were significantly greater than those of the remaining materials.

The observations permit the conclusion that each of the Japan-produced materials have a high resistance to embrittlement by 288°C irradiation. Additionally, they showed a greater resistance to radiation than the IAEA reference plate. In this regard, the somewhat poorer performance of the reference plate can be attributed to its higher copper content (i.e., .12%Cu versus .04%Cu, Japan-produced materials).

Future Plans

Plans for the coming quarter include completion of PCC_v specimen evaluations of pre- and postirradiation conditions. It is also expected that the materials produced in France and Germany (now in transit) will be received at NRL. Specimen blanking operations are planned for late FY-79.

TABLE I

Identification of Test Materials

Material/ Producer	Codes	Thickness (cm)	Chemical Composition (wt.%) C	Mn	Si	P	S	Ni	Cr	Mo	Cu	Heat Treatment
HSST A533-B Plate 03 (Lukens Steel)	3MU, 3NE	30.5	.20	1.26	.25	.011	.018	.56	.10	.45	.12	1
Japan A533-B Plate (Nippon Steel)	107	25.1	.18	1.48	.22	.007	.007	.66	.20	.57	.01	2
Japan A508-3 Forging (Japan Steel)	212, 213	30.2	.18	1.35	.27	.007	.005	.76	.12	.49	.04	3
Japan S/A Weld (Mitsubishi)	502, 503	24.8	.07	1.20	.32	.008	.003	.89	.06	.50	.04	4
Japan A533-B Plate (Parent Plate Weld 502)	LG	24.5		5		(Not Available)						

Heat Treatments:

1. 843 to 899°C - 4 hr, WQ; 649 to 677°C - 4hr, AC; 607 to 635°C - 20 hr,FC.
2. 880°C - 8 hr, WQ; 660°C - 6 hr, AC; 620°C - 26 hr, FC.
3. 870 to 900°C - 6.4 hr, WQ; 635 to 645°C - 7.8 hr, AC.
4. (PWHT) - 615°C - 26 hr, FC.
5. Not known.

TABLE 2

Tensile Properties of the Test Materials*

(Unirradiated Condition at 24°C)

Material Codes	YS (MPa)	TS (MPa)	RA (%)	Elong. (%)
HSST 03	464	628	65.0	25.3
JP 107	442	589	72.6	24.7
JF 212	462	597	70.7	26.2
JW 502	530	619	73.0	24.8
JW(BP) LG	444	581	72.6	28.8

*Average, duplicate tests.
TL orientation, plate and forging.

TABLE 3

Summary of Preirradiation and Postirradiation

Charpy-V Notch Ductility Properties of Test Materials

Material	Transition Temperature C_v 41J (°C)			Transition Temperature C_v 68J (°C)			C_v 0.9 mm (°C)			Upper Shelf Energy (J)			Upper Shelf Lateral Expansion (mm)		
	Initial	Irrad.	Change	Initial	Irrad.	Change	Initial	Irrad.	Change	Initial	Irrad.	Change	Initial	Irrad.	Change
HSST 03	- 1	43	44	29	76	47	24	80	56	138	136	∿0	2.0	1.6	0.4
JP 107	-46	-29	17	-35	-21	14	-38	-21	17	> 270	212	≥ 58	2.3	2.1	0.2
JP 212	-63	-32	31	-54	-21	33	-54	-21	33	∿ 233	∿218	∿ 15	∿2.1	∿ 2.0	∿ 0.1
JW 502	-42	-23	19	-29	-12	17	-34	- 7	28	184	184	∿ 0	2.2	2.0	0.2
JW(BP) LG	-37	-23	14	-32	-15	17	-34	-15	19	> 270	-228	≥ 37	2.2	1.9	0.3

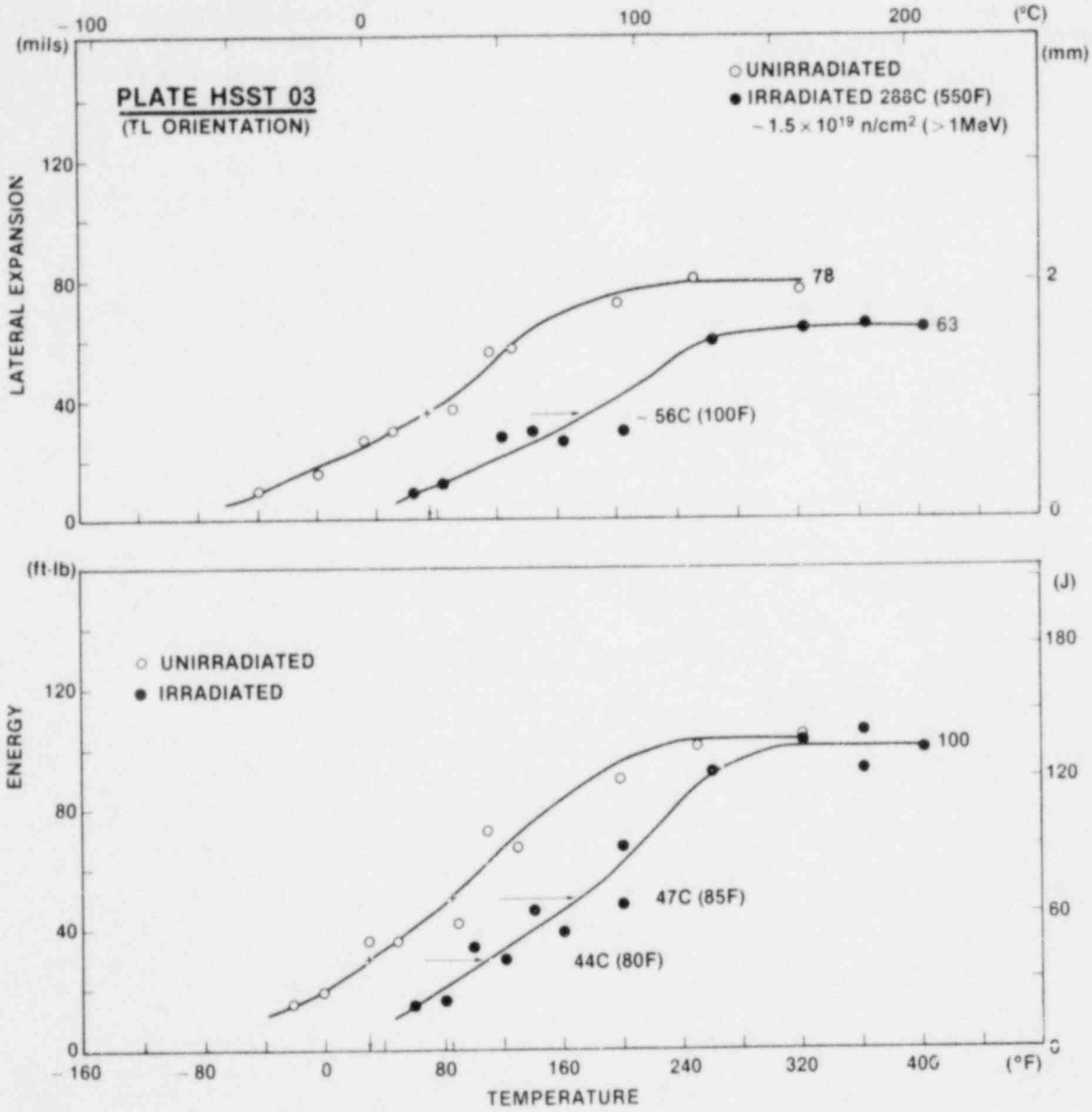

Fig. 1 Charpy-V notch ductility of the United States-produced A533-B steel plate (HSST Program Plate 03) before and after irradiation. In this figure, and in Figures 2 through 5, the upper graph relates specimen lateral expansion and temperature while the lower graph relates specimen energy absorption and temperature.

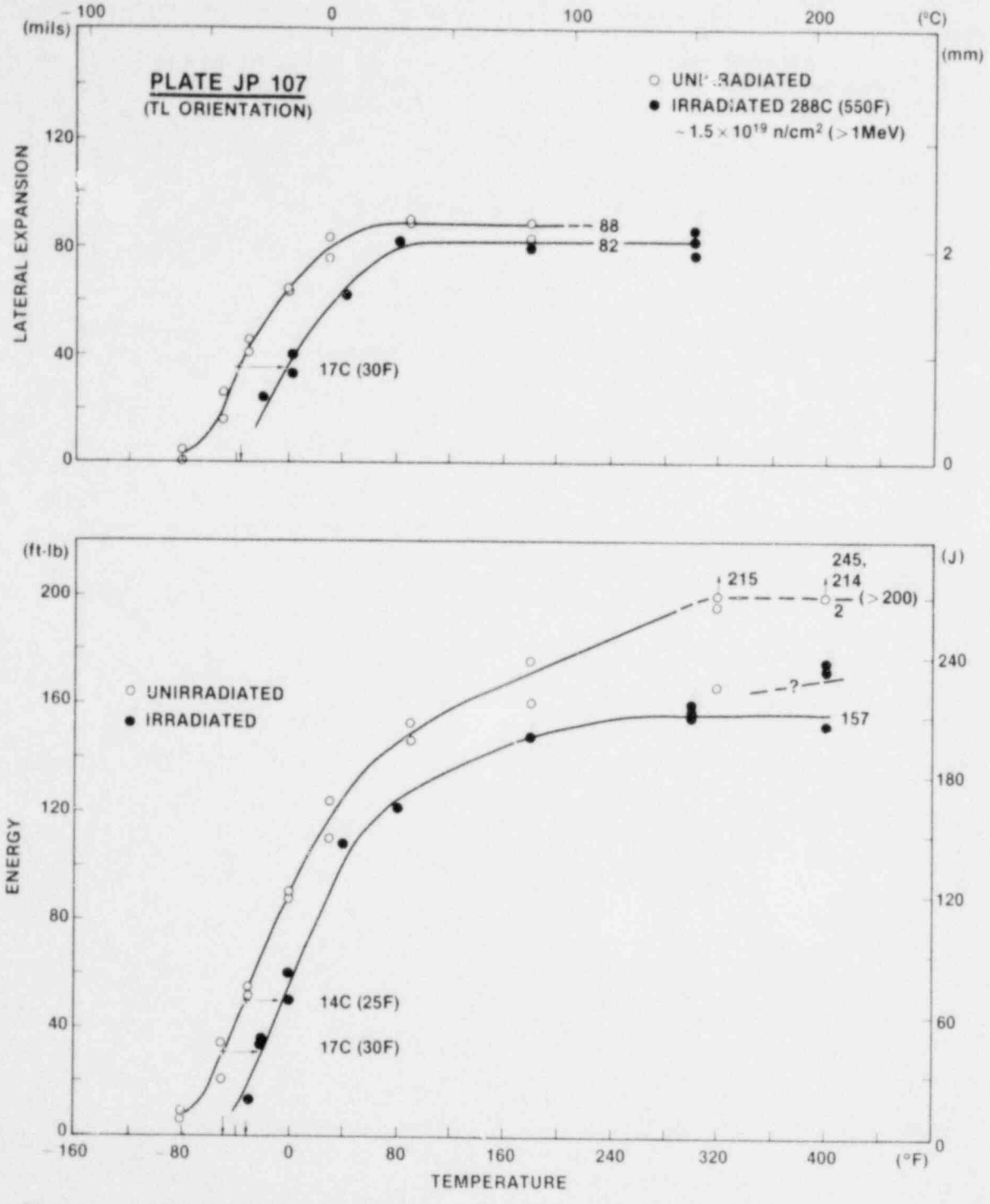

Fig. 2 Charpy-V notch ductility of the Japan-produced A533-B steel plate, Code JP 107.

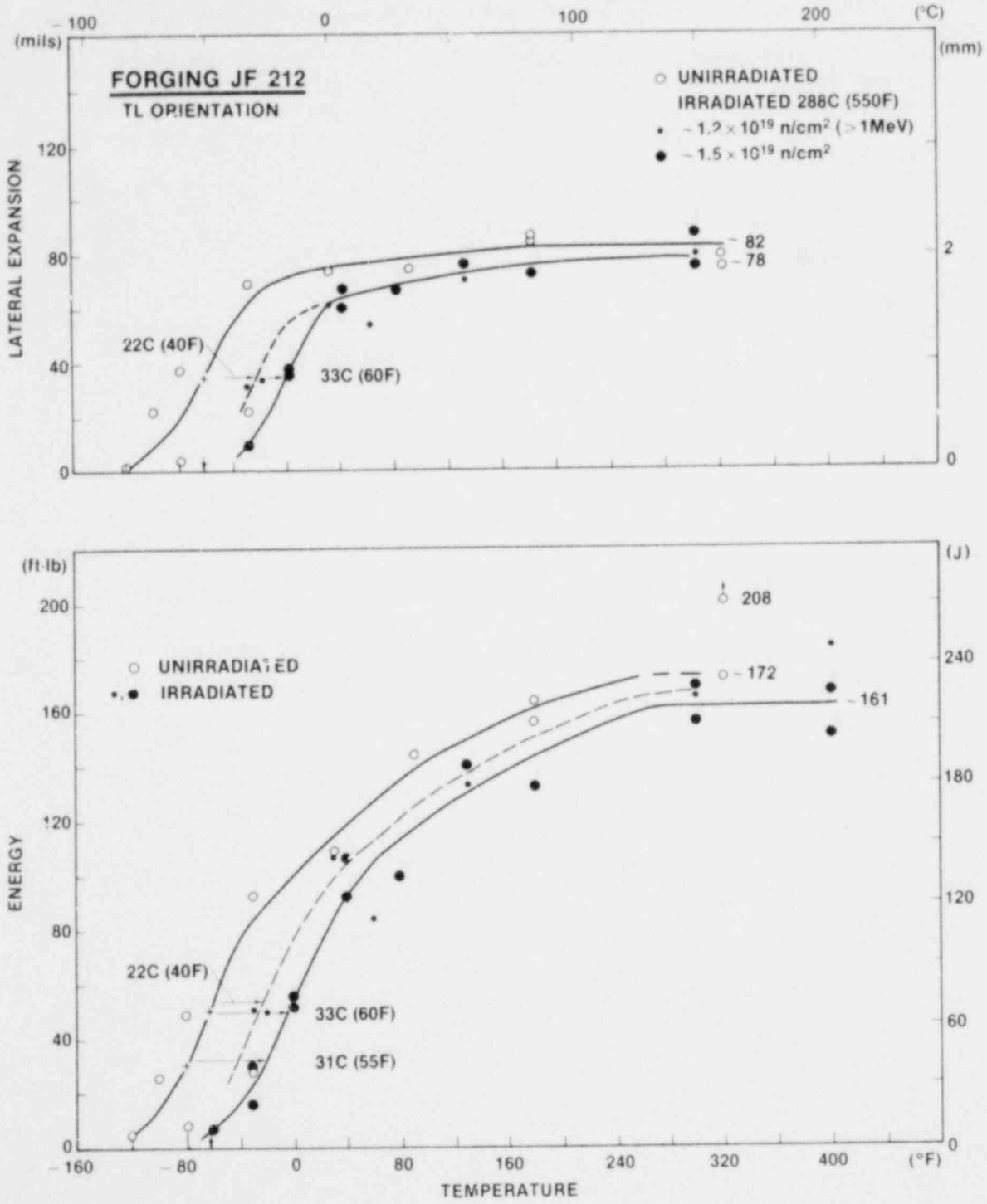

Fig. 3 Charpy-V notch ductility of the Japan-produced A508 Class 3 forging, Code JF 212. Results for two irradiation experiments are indicated.

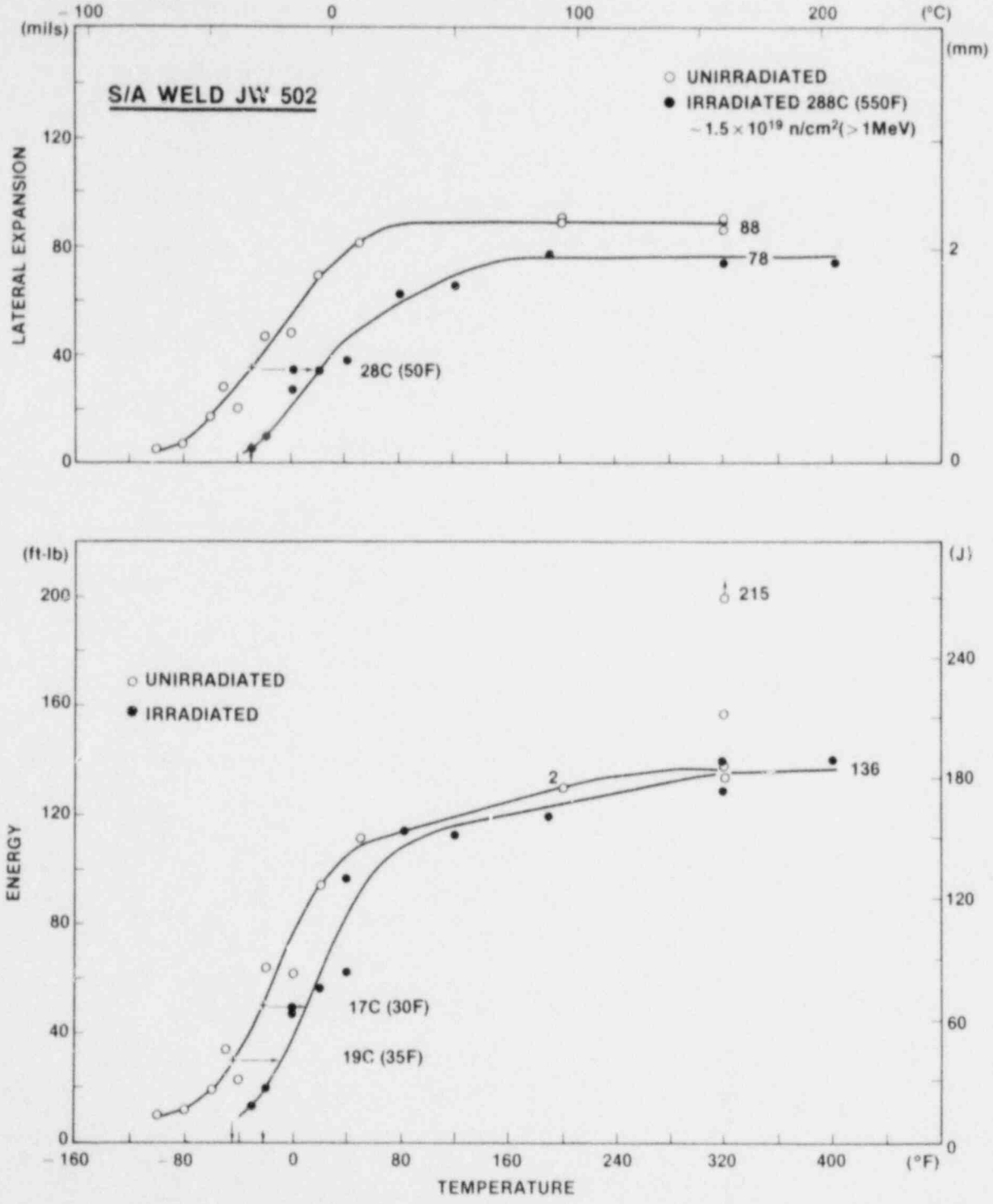

Fig. 4 Charpy-V notch ductility of the Japan-produced submerged arc weld deposit, Code JW 502. The specimens were oriented with their long dimension perpendicular to the welding direction and parallel to the weldment surface.

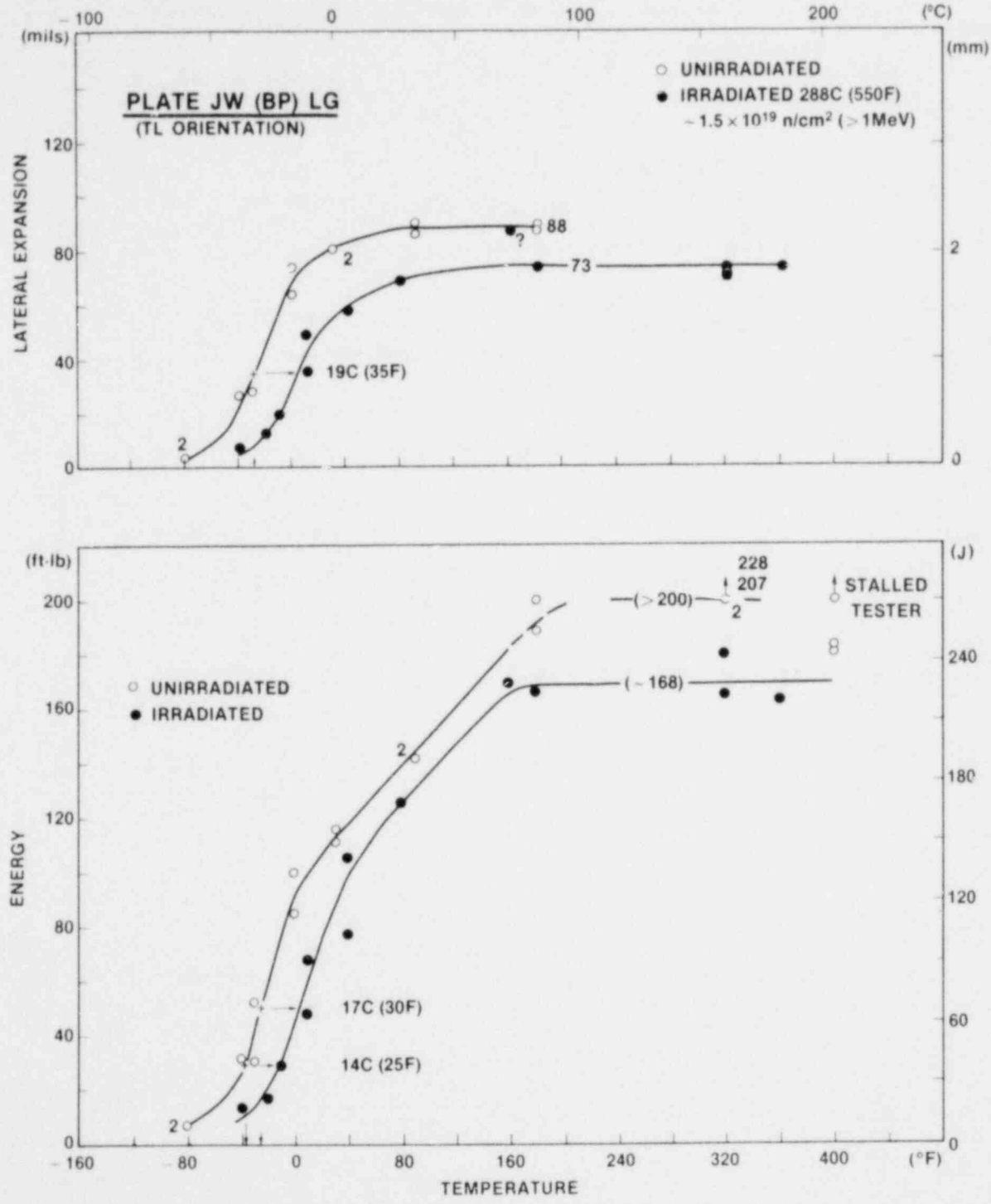

Fig. 5 Charpy-V notch ductility of the Japanese-produced A533-B plate, Code LG. This matrial was the base plate for weld JW 502 (see Fig. 4).

B. IAR Program Investigations of Charpy-V Notch Ductility Trends With Cyclic Postirradiation Annealing and Reirradiation Treatments

J. R. Hawthorne, H. E. Watson, and F. J. Loss

Background

The IAR Program is investigating the notch ductility behavior of submerged arc weld deposits with irradiation (I) followed by two full cycles of postirradiation annealing (A) and reirradiation (R). The intent of the program is to identify the merits and potential of the method for control of radiation-induced embrittlement in reactor pressure vessels.

In a previous progress report [4], the background and objectives of the program were outlined. The planned experimental test matrix (Table 4) was also discussed together with a description of the materials selected for study (Table 5). Findings from Experiments 1 and 2 on IA, IAR and IARA trends have been reported [5]. In brief, the results of these experiments revealed that a 343°C (650°F) intermediate heat treatment may not be a practical method for the control of radiation embrittlement in reactor vessels because of the high frequency of annealing which would be required. A 399°C (750°F) heat treatment, on the other hand, showed definite promise for the control of radiation effects buildup in vessels. That is, both welds showed better notch ductility after 399°C annealing and reirradiation than after the first cycle of radiation exposure (see Figs. 6 and 7). Based on this finding, 399°C (750°F)-168 hr annealing conditions were selected for investigation in Experiments 3 and 4 (Table 4). In addition, the target reirradiation fluence was selected to be $\sim 0.6 \times 10^{19}$ n/cm^2 >1 MeV.

Reactor irradiation operations for Experiments 3 and 4 have now been completed. Postirradiation Charpy-V tests to evaluate IARAR performance (two complete intermediate annealing and reirradiation treatments) have also been completed and are reported here.

Progress

Charpy-V (C_v) notch ductility determinations for the IARAR condition of welds V86 and V84 are shown in Figs. 8 and 9 respectively. Weld properties after the initial radiation exposure (curve I) and after the second intermediate 399°C (750°F)-168 hr annealing treatment (curve IARA) are also shown for reference. Neutron dosimetry results are not yet available; however, the fluences received during the first radiation cycle (I) and by the second and third (repeat) irradiation cycles (R) are estimated at 1.2, 0.7, and 0.7 x 10^{19} n/cm^2 (> 1 MeV) respectively. Accordingly, the total fluence received by the IARAR condition is estimated at 2.6 x 10^{19} n/cm^2.

Several important observations are permitted by the new data. First, the results clearly demonstrate the benefits of intermediate 399°C (750°F) annealing and that the benefits can be retained through two cycles of reirradiation. Specifically, the upper shelf level of the IARAR condition is significantly higher, in each case, than that of the I condition of the weld. At the same time, the C_v

TABLE 4

Radiation Experiment Matrix
288°C (550°F) Irradiation

Experiment Number	Specimen Types	Designation	Objective
1	C_v	IA	Explore recovery by 343 and 399°C (650 and 750°C) annealing
2	C_v	IAR	Explore reirradiation response of all three materials
3	CT, C_v	I through IARAR	Determine IARAR performance of Weld 1
4	CT, C_v	I through IARAR	Determine IARAR performance of Weld 2

TABLE 5

Chemical Compositions of IAR Program Welds

Material	Code	Weight (%) Cu	C	Mn	Si	P	S	Ni	Mo	V	Cr
S/A Weld 1 (Linde 1092 flux)	V84	.35	.14	1.56	.14	.013	.011	.62	.53	.002	.03
S/A Weld 2 (Linde 80 flux)	V86	.35	.08	1.60	.55	.016	.013	.69	.40	.006	-

Heat Treatment	V84	Stress relief annealed 593 to 621 ^{o}C - 50 hr, furnace cooled to 316 ^{o}C at 6 ^{o}C/hr, air cooled.
	V86	Stress relief annealed 621 ^{o}C - 40 hr, furnace cooled to 316 ^{o}C.

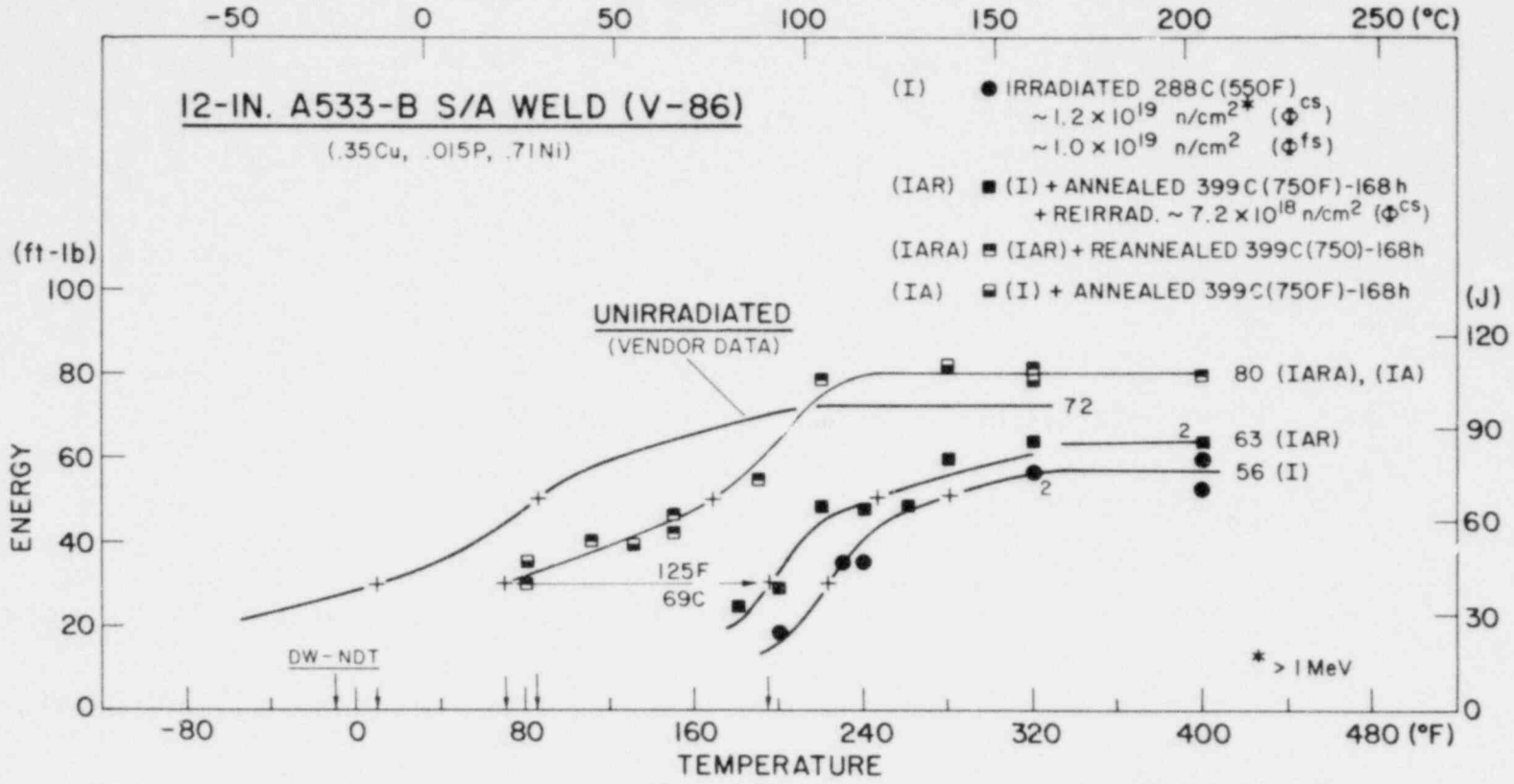

Fig. 6. Notch ductility behavior of weld V86 after reirradiation following a 399°C (750°F)-168 hr annealing heat treatment (curve IAR) and after reirradiation and re-heat treatment at 399°C (curve IARA). The notch ductility of the weld after the first cycle of irradiation (curve I) and after the first cycle heat treatment (data points IA) are also shown for reference [5].

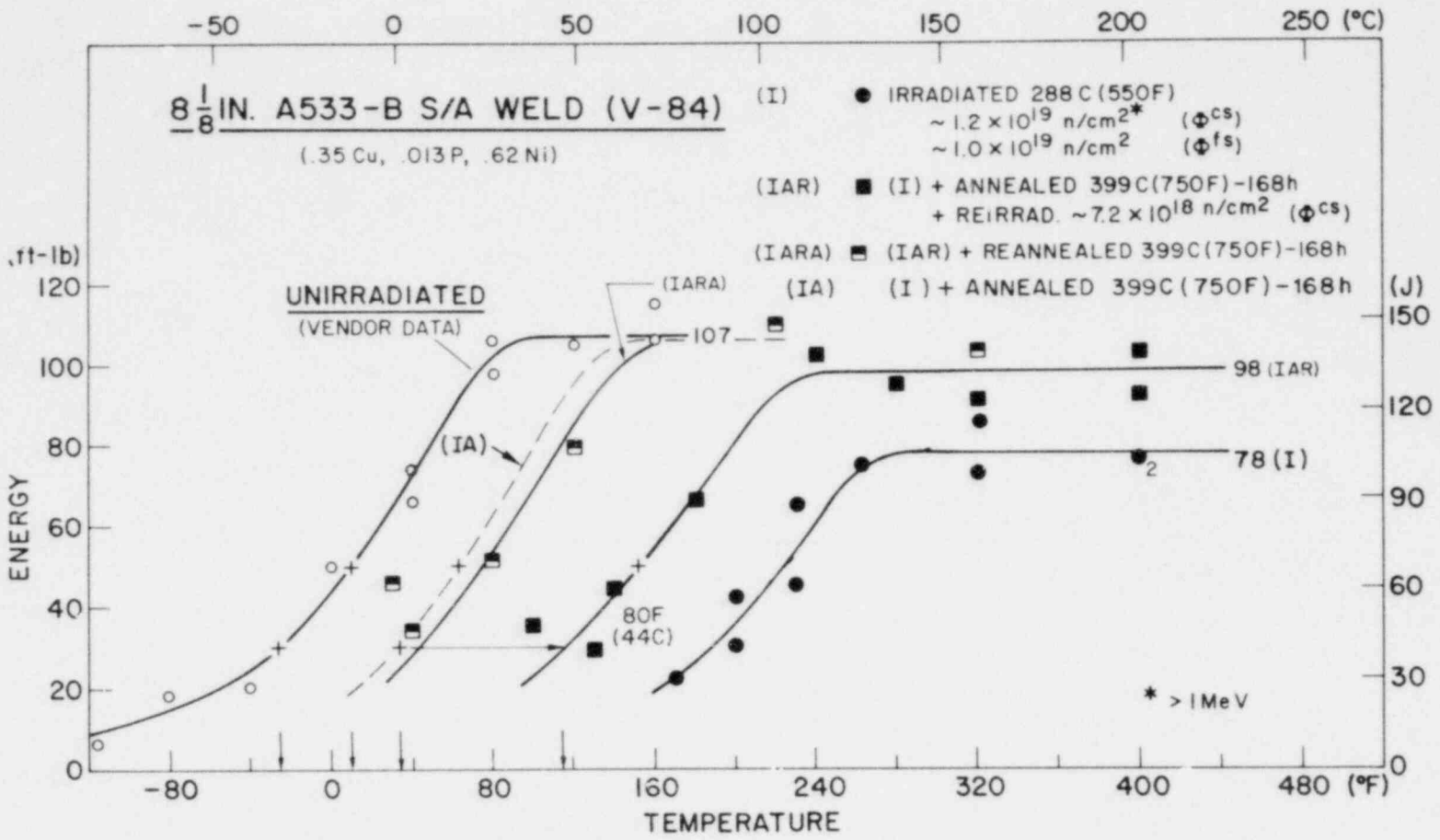

Fig. 7 Notch ductility behavior of weld V84 after reirradiation following a 399°C (750°F)-168 hr annealing heat treatment (curve IAR) and after reirradiation and re-heat treatment at 399°C (curve IARA). The notch ductility of the weld after the first cycle of irradiation (curve I) and after the first cycle heat treatment (curve IA) are also shown.

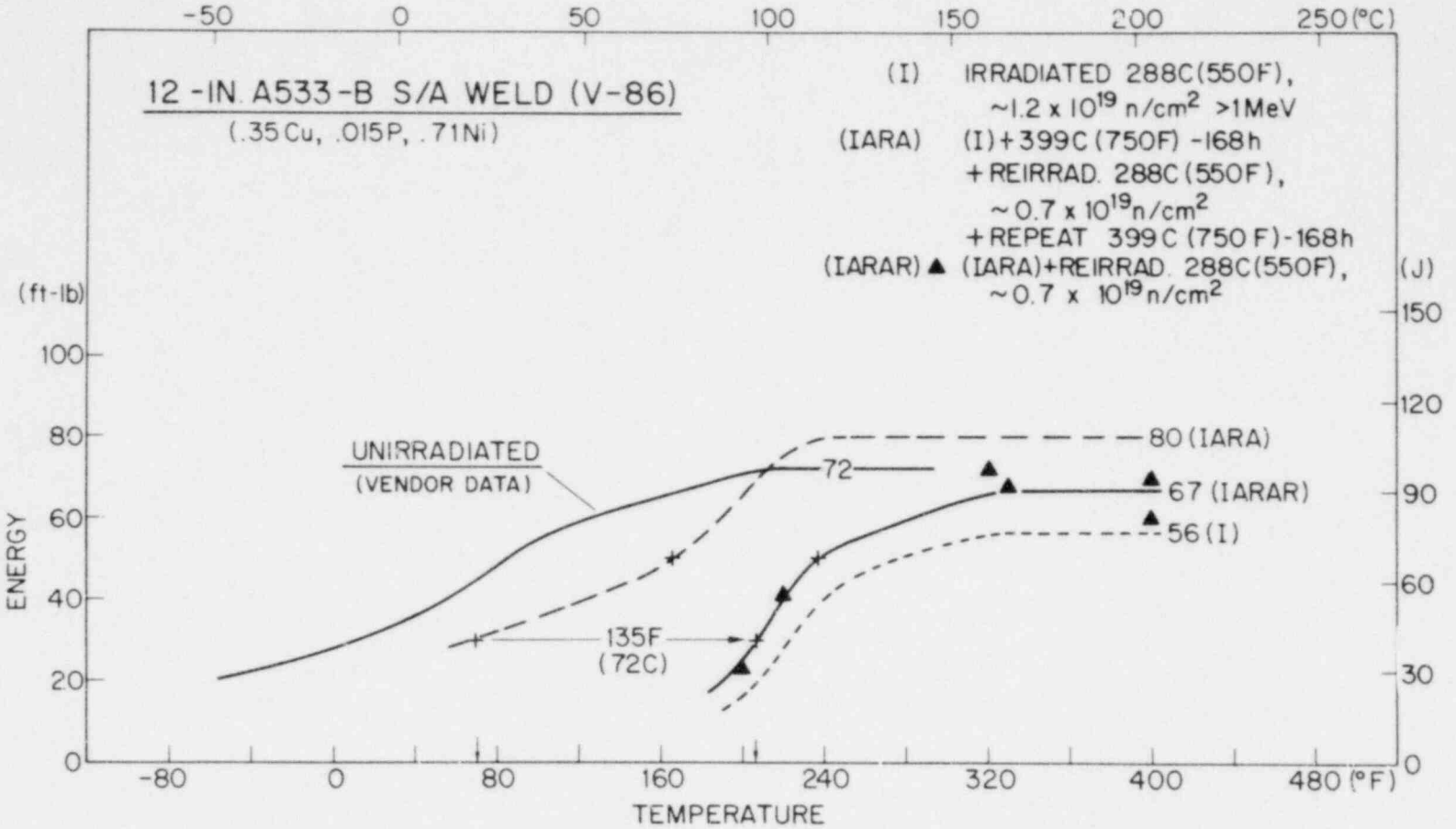

Fig. 8 Charpy-V notch ductility of weld V86 after two cycles of intermediate 399°C (750°F)-168 hr annealing and 288°C (550°F) reirradiation. The dashed curves labeled (I) and (IARA) represent the first cycle irradiation and second cycle annealed conditions respectively. A significant benefit of cyclic irradiation and annealing to notch ductility retention is indicated.

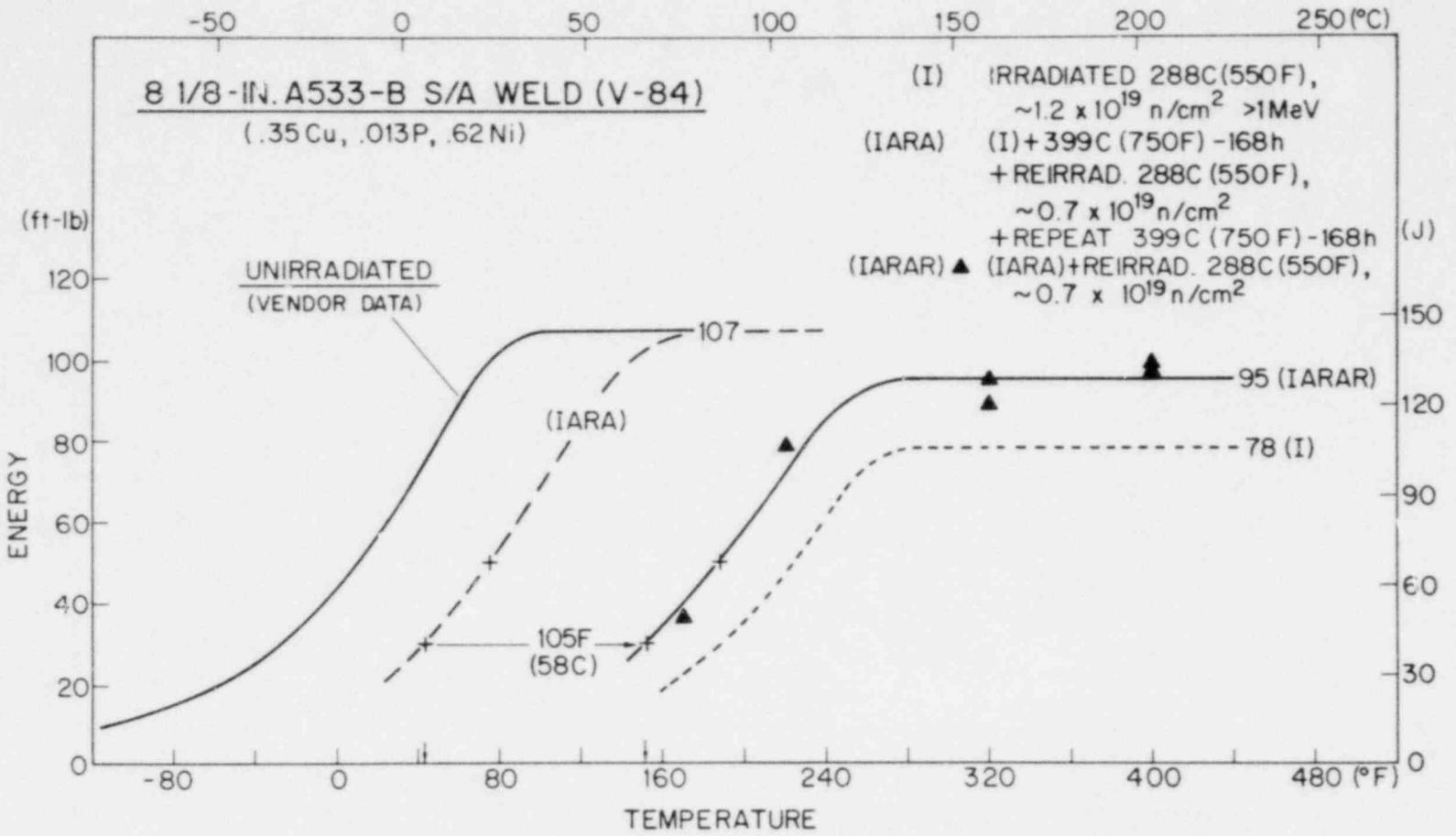

Fig. 9 Charpy-V notch ductility of weld V84 after two cycles of intermediate 399°C (750°F)-168 hr annealing and 288°C (550°F) reirradiation. Curves (dashed) showing properties of the (I) and (IARA) conditions are also shown.

41J transition temperature for the IARAR condition is significantly lower than that of the I condition. Second, the results confirm the earlier observation (5) for the IAR condition that the rate of reembrittlement of annealed material is higher than that of non-annealed material for the same increment of additional fluence. Third, the upper shelf reduction and transition temperature elevation experienced by the welds during the third cycle of irradiation appear to be about the same as those changes observed for the second cycle of irradiation (compare IARAR and IAR conditions of Figs. 8 and 6 and of Figs. 9 and 7). If additional data confirm this tentative indication, it would appear that notch ductility changes can be maintained below prefixed limits by carefully selected annealing schedules for individual materials. Moreover, the results indicate a good possibility for optimizing annealing schedules once the effectiveness of 399°C (750°F) annealing, in terms of residual embrittlement after an anneal, and the material reembrittlement rate is established. The acquisition of further insight into such factors is an important objective of the continuing IAR Program.

Status and Future Plans

A report providing a complete review and summary of the Phase 1 C_v investigations by the IAR Program is in preparation. The report will include information on hardness and lateral expansion trends observed for the welds during cyclic annealing and reirradiation as well as energy trend information. Tests of the compact toughness (CT) specimens included in experiments 3 and 4 have commenced; discussion of observations thus far are reported in a subsequent section.

Phase 2 investigations have also commenced with the procurement of additional weld metal stock comparable to welds V86 and V84. Phase 2 objectives include but are not limited to determinations of notch ductility trends as functions of first and second cycle fluence levels, reembrittlement rate as a function of fluence, and time-temperature relationships in recovery. Phase 2 studies also will continue the present investigation on the correlation of notch ductility and fracture toughness for irradiated, annealed and reirradiated conditions.

II. FRACTURE MECHANICS INVESTIGATIONS

A. J-R Curve Characterization of Irradiated Submerged Arc Weld Deposit

F. J. Loss, B. H. Menke, R. A. Gray, Jr., J. R. Hawthorne, and H. E. Watson

Background

An integral part of the IAR program described in the preceding section involves the development of J-R curve trends for the two submerged arc weld deposits listed in Table 5. This study employs compact (CT) specimens of 25.4 mm (1 in.) thickness to characterize the toughness changes with irradiation. Two full cycles of annealing and reirradiation are being investigated as a counterpart to the C_v investigations. The primary objective is to define the J_{Ic} and R curve behavior in the upper shelf temperature regime. Here, a correspondence is being developed between changes in the J-R curve and in C_v upper shelf energy as a function of irradiation and annealing. If successful, this relationship will provide added quantitativeness to surveillance programs which may involve only C_v specimens. As a secondary objective, an estimate of the temperature elevation of the brittle/ductile transition region with irradiation is being made on the basis of only a few J_{Ic} tests. This temperature elevation, based on static tests, will be compared with a similar change based upon the (dynamic) C_v tests.

The J-R curves are measured by means of the single specimen compliance (SSC) technique using 1T-CT specimens which have been fatigue precracked to a crack length, a, to width, W, ratio of 0.6. A large part of the program has centered on the development of procedures to assure adequate definition of crack extension, Δa, using this technique as well as to develop methods for the hot-cell testing of irradiated specimens. In addition, a related study on specimen side groove depth was undertaken to characterize the influence of this variable on crack-front straightness and the resulting effect on R-curve slope.

Progress to date has included the successful implementation of the SSC technique for irradiated specimen testing. In addition, characterization of specimens from one A533-B weld deposit, Code V86, in the I, IAR, and IARAR conditions has been completed. These results represent the first application of the SSC technique to irradiated material.

Experimental Procedure

With the SSC technique it is necessary to achieve a partial unloading of the specimen (e.g., 10 percent) such that the unload-reload records of load, P, versus deflection, δ, enable the specimen compliance δ/P to be defined. Examples of the procedure are illustrated in Figs. 10 and 11. The standard 1T-CT specimen geometry has been modified (Fig. 12) to permit the attachment of razor knife edges for the measurement of load-line displacement with a clip gage. An experimental compliance for both smooth and 25 percent side-grooved specimens has been developed with 1T-CT specimens (Fig. 13). With this

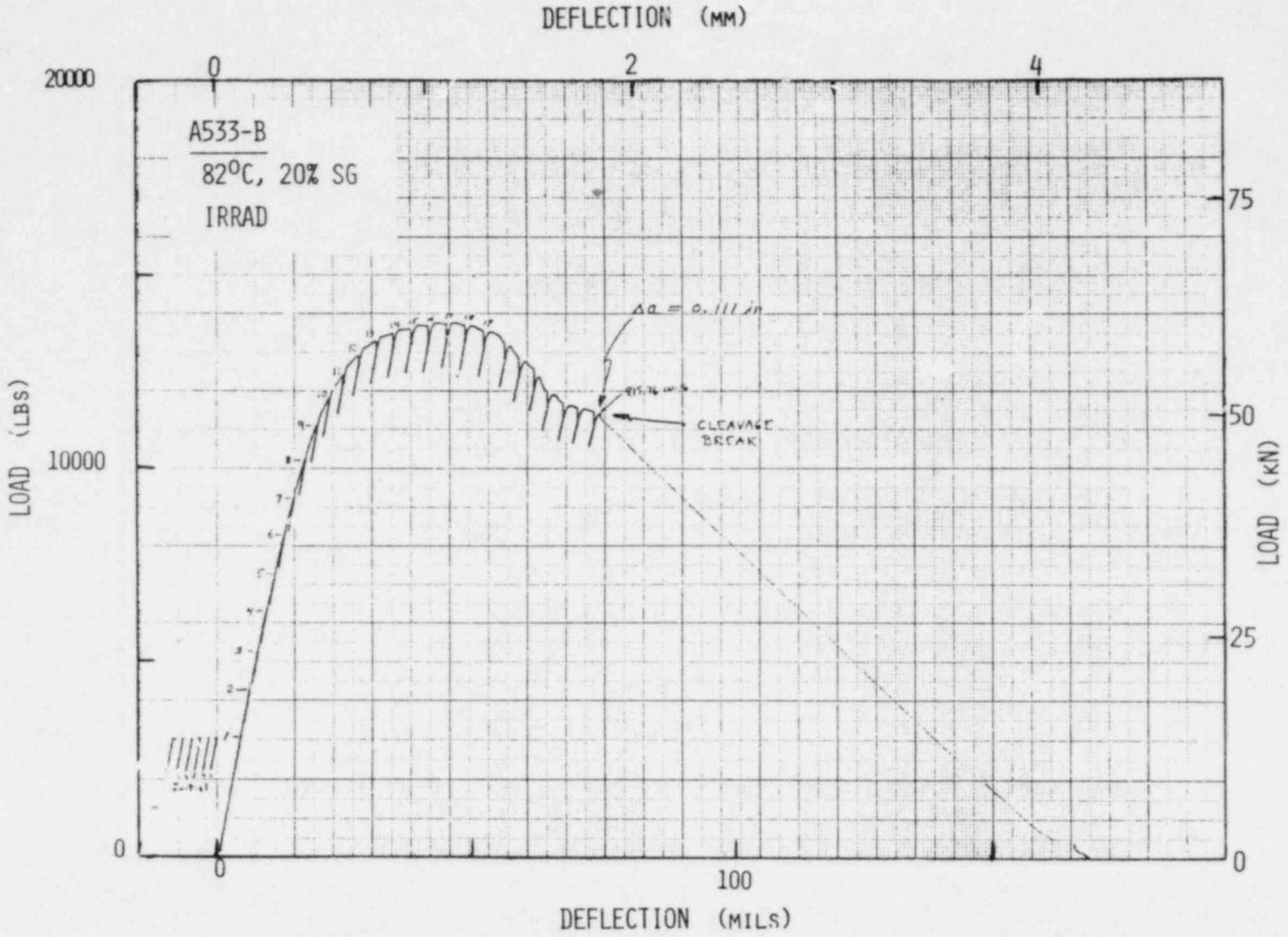

Fig. 10 Example of load vs load-line deflection record from the test of a 1T-CT specimen in the irradiated condition. A levelling of the curve is indicated just prior to unstable fracture.

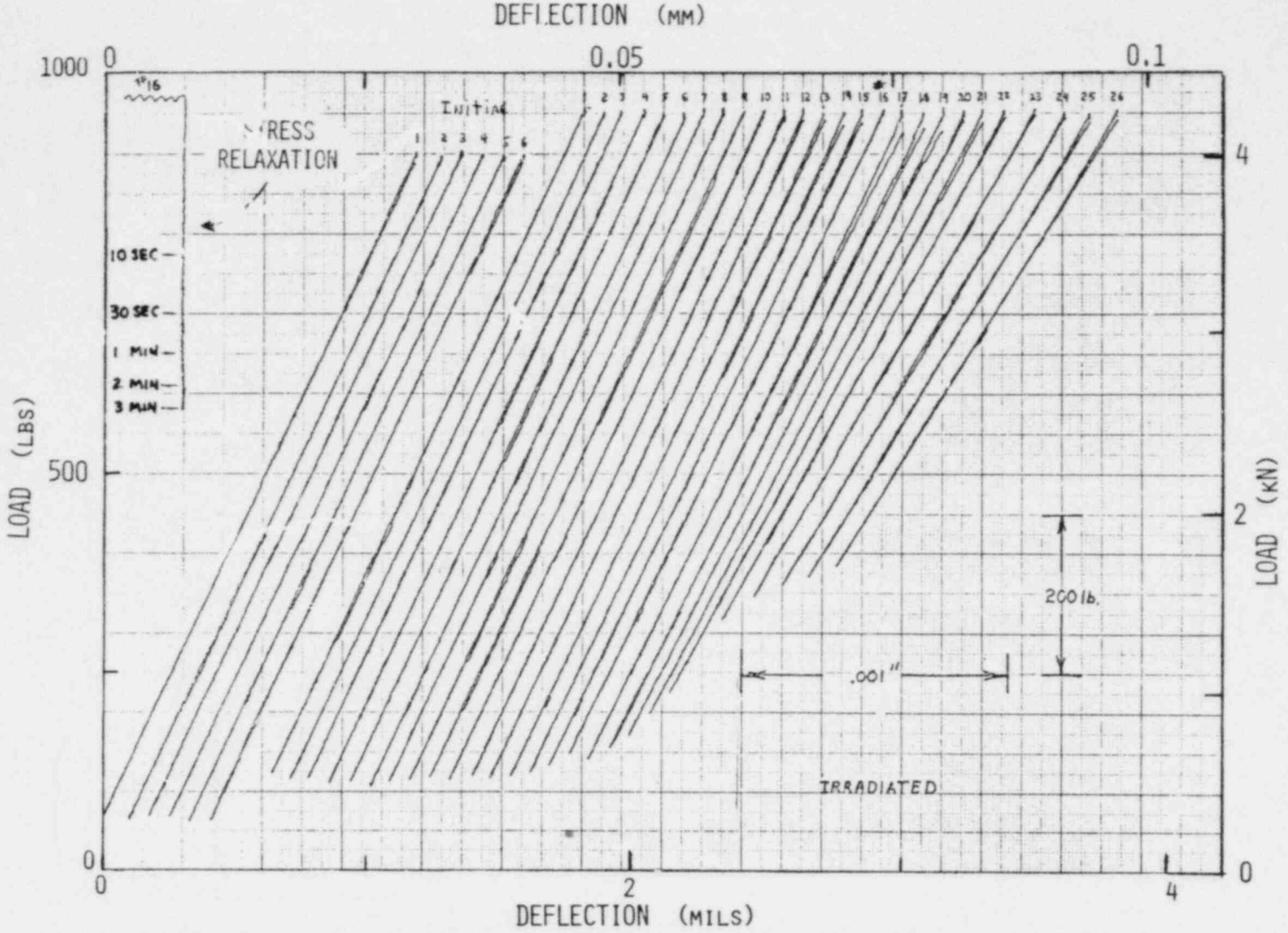

Fig. 11 Highly amplified unload-reload traces of the irradiated test illustrated in Fig. 10. Note the absence of hysteresis. Also shown is an example of the material relaxation behavior (upper left) for unloading No. 16.

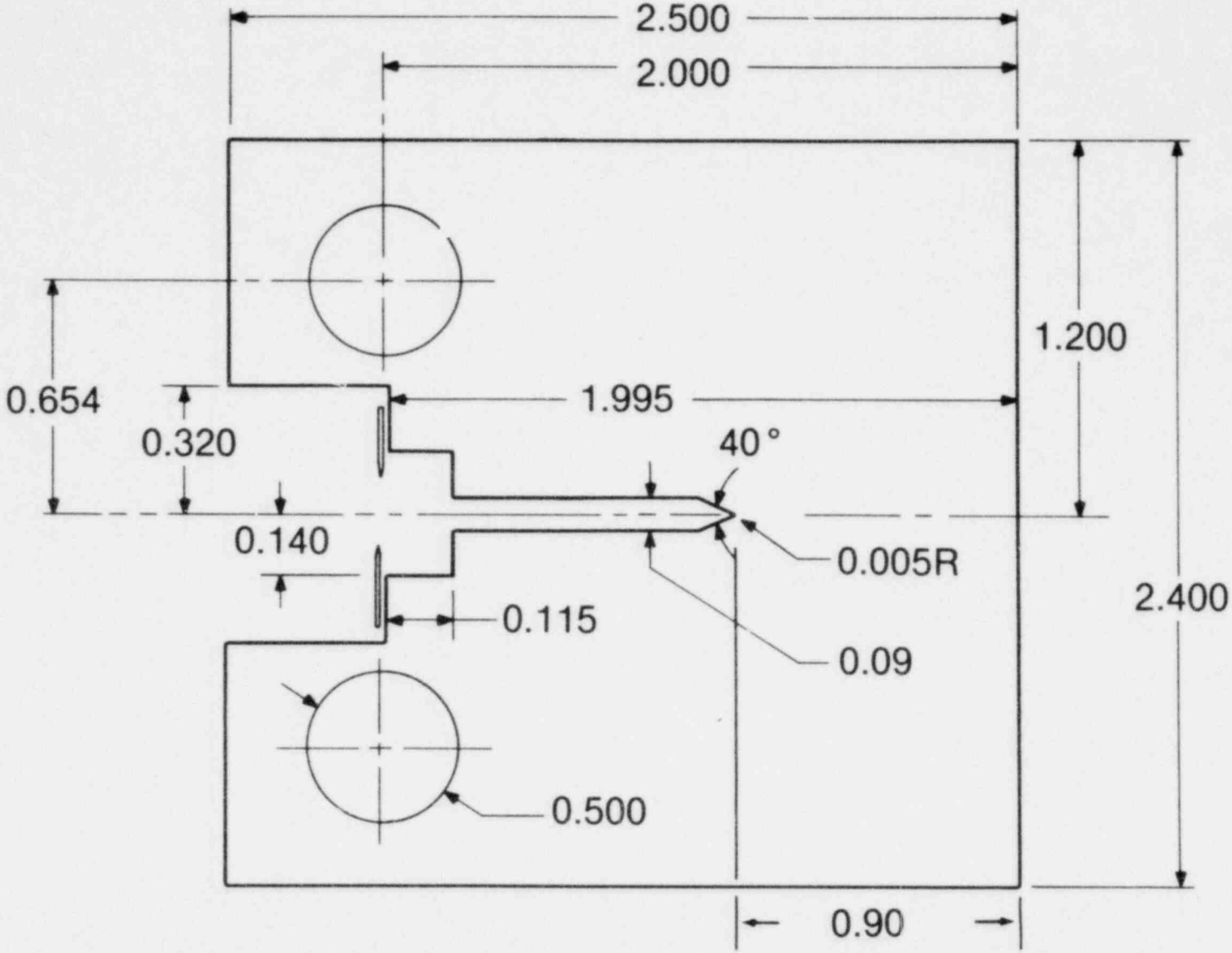

Fig. 12 1T compact specimen geometry for an a/W of 0.6. A precrack of 2.5 mm (0.100 in.) is added prior to testing. All dimensions are in inches (in. x 25.4 = mm).

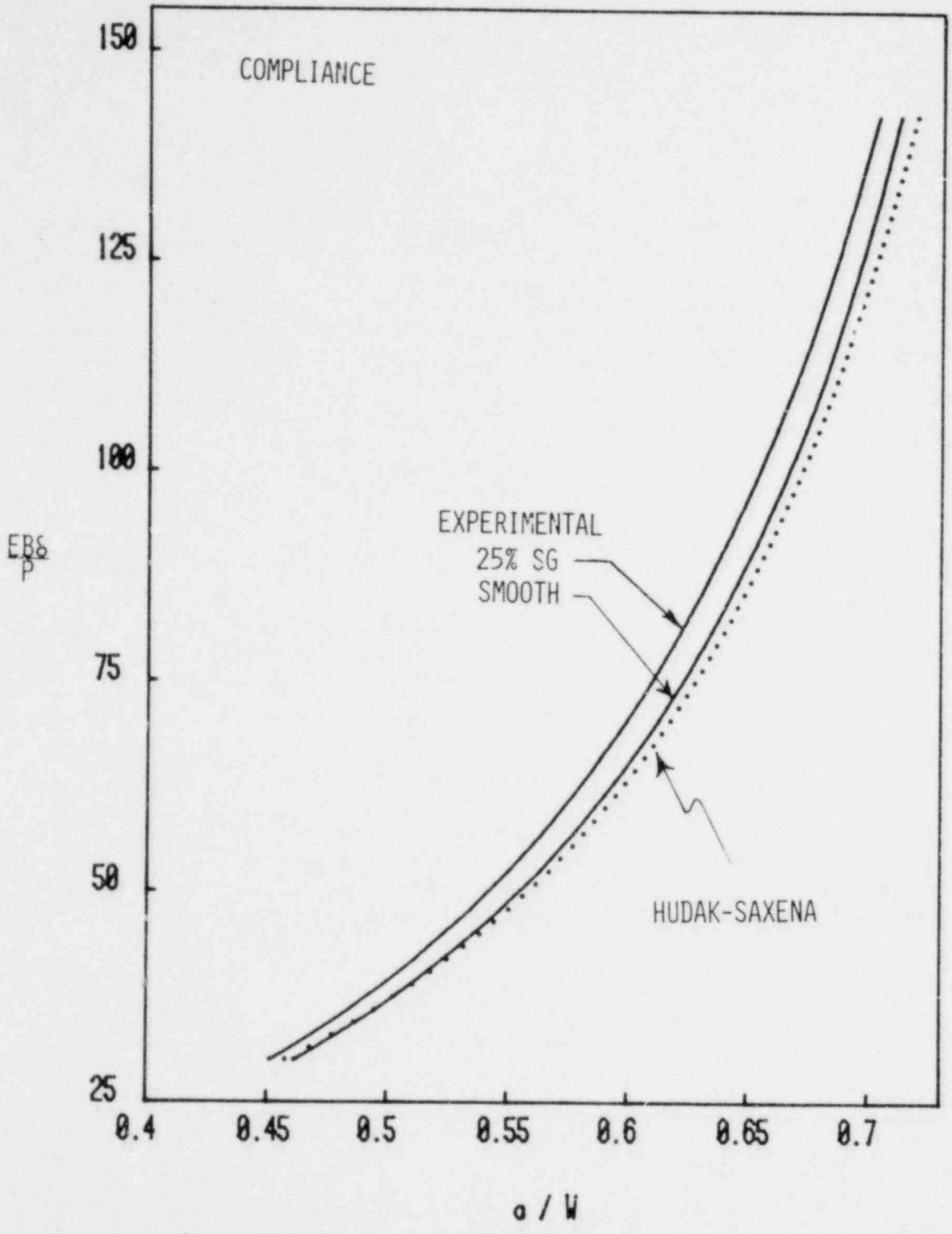

Fig. 13. Comparison of the CT specimen compliance derived analytically using a plane stress assumption (Hudak-Saxena) with that measured experimentally with blunt-notch specimens (smooth). The two curves have been "matched" at an a/W of 0.5. Also illustrated is the experimental compliance for specimens having 25% side grooves (25% SG).

relationship crack length changes can be inferred from the measured changes in specimen compliance. Note that the experimental compliance for smooth specimens shown in Fig. 13 differs only slightly from the theoretical expression of Hudak and others [6] based upon a plane stress assumption.

Successful application of the SSC technique relies upon accurate crack length predictions. This, in turn, requires the minimization of both friction and electronic noise so that the specimen compliance can be established with precision. The experimental record of Fig. 11 is typical of a highly amplified unload/reload test sequence to determine compliance changes. From a repeatability viewpoint, the initial four unloadings in this record are sufficiently accurate to define the crack length to a precision of $\pm$ 0.05 mm (2 mils) in a 1T-CT specimen with a 95 percent confidence limit. However, repeatability is not to be confused with accuracy. The latter is difficult to define exactly because of its dependence on the compounding of errors due to load cell and clip gage calibration factors, modulus determination, validity of the compliance expression and variations caused by the electronic noise level. Nevertheless, our development of the SSC method has resulted in test records which exhibit a scatter of only $\pm$ 0.08 mm ($\pm$3 mils) in the predicted crack length in a 1T-CT specimen. As a test of this predictive capability a correspondence between the predicted and the optically-measured final crack lengths, when these crack fronts are straight, is typically within $\pm$0.13 mm ($\pm$5 mils) (see Table 6). On the other hand, larger discrepancies between predicted and measured crack extensions have been detected for smooth specimens having curved or tunneled crack fronts; the same is true of specimens which have been machined from an A302-B steel plate having a high non-metallic inclusion content [7] even though straight crack fronts were exhibited.

The magnitude of J is computed from the relationship:

$$J = \frac{1+\alpha}{1+\alpha^2}\,\frac{2A}{\left[B_n b_o\right]} \qquad (1)$$

where A is the specimen energy absorbed based on total deflection, b_o is the original unbroken ligament, B_n is the net thickness and the term $(1+\alpha)/(1+\alpha^2)$ is a modified Merkle-Corten correction to account for the tension component of the loading [8]. A correction [7] is also applied to account for minor specimen rotation which occurs during loading. This rotation reduces the moment arm of the load and also results in a deviation of the clip gage loading points from the true load line. A computer is used to provide on-line determinations of J and crack extension, Δa. The computer code was originally developed by Joyce and Gudas [9].

J_{Ic} Measurement Procedure

Figure 14 illustrates a typical J-R curve for the weld metal (Code V86) at a temperature within the upper shelf regime. The J_{Ic} value is currently defined by the proposed ASTM multispecimen standard [10] as the intersection of the blunting line ($\Delta a = J/2\sigma_f$) with the least-squares fit of the points lying between lines 1 and 2 illustrated in the figure. Line No. 1 is drawn parallel to the blunting line at a crack extension of 0.15 mm. This is termed an "exclusion line" and is

TABLE 6

Toughness Properties of A533-B Submerged Arc Weld Deposit

Specimen Number	% Side Grooves	Irrad. Condition[a]	Test Temp °C (°F)	J_{Ic} kJ/m² (lb/in.)		T^b	T^c	Δa Measured mm	(mils)	Δa Predicted mm	(mils)	a/W	$25J_{Ic}/\sigma_f$ mm	(in.)	ω^d
V86-18	0	I	200 (392)	79	(450)	43	33	5.9	(231)	4.0	(158)	0.60	3.2	(0.13)	21
-21	10	I		80	(455)	21	14	9.1	(360)	9.1	(357)	0.61	3.3	(0.13)	9
-27	20	I		66	(375)	28	15	8.5	(334)	8.5	(332)	0.61	2.7	(0.11)	14
-13	20	I		65	(370)	24	17	5.9	(231)	5.9	(232)	0.61	2.7	(0.11)	14
- 5	20	IAR		72	(410)	30	19	6.5	(255)	6.5	(258)	0.62	2.9	(0.12)	15
- 4	20	IAR		77	(440)	34	20	8.6	(339)	8.7	(339)	0.61	3.1	(0.12)	17
- 2	20	IARAR		71	(405)	32	22	4.9	(194)	5.0	(199)	0.61	2.9	(0.11)	17
- 8	0	IARAR	38 (100)	44	(249)	-	-	-	-	-	-	0.61	-	-	-
-24	20	U	-100 (-148)	23	(130)	-	-	-	-	0.1	(3)	0.62	1.1	(0.04)	-
-28	20		-72 (-98)	38	(217)	-	-	0.0	(1)	0.0	(1)	0.61	1.8	(0.07)	-
-31	20		-60 (-76)	62	(356)	-	-	-	-	0.1	(4)	0.62	3.0	(0.12)	-
-29	20		-50 (-58)	89	(510)	-	-	0.1	(3)	0.2	(6)	0.62	4.3	(0.17)	-
-17	20		-40 (-40)	119	(681)	-	-	0.2	(6)	0.2	(7)	0.61	5.7	(0.23)	-
- 1	20		-11 (12)	119	(682)	-	-	0.2	(6)	0.2	(6)	0.64	5.8	(0.23)	-
-30	20		20 (68)	124	(710)	103	64	4.7	(184)	4.7	(186)	0.62	6.1	(0.24)	17
- 3	20		200 (392)	123	(705)	70	53	4.0	(159)	4.0	(156)	0.62	6.4	(0.25)	14
-26	0		200 (392)	132	(755)	116	-	2.2	(87)	1.8	(70)	0.61	6.8	(0.27)	23
-15	10		200 (392)	144	(820)	102	72	4.1	(162)	3.5	(139)	0.61	7.4	(0.29)	17

[a] U = Unirradiated
I = Irrad, 1.2×10^{19} n/cm²
A = Annealed 399°C (750°F), 168 hr
R = Reirradiation, 0.7×10^{19} n/cm²

[b] $T = \frac{E}{\sigma_f^2} \frac{dJ}{da}$; uses least squares slope of R curve and 1.5 mm Δa

[c] Evaluated at Δa = 1.5 mm plus blunting and using instantaneous dJ/da

[d] $\omega = \frac{b}{J_{Ic}} \frac{dJ}{da}$; uses least squares slope of R curve and 1.5 mm Δa

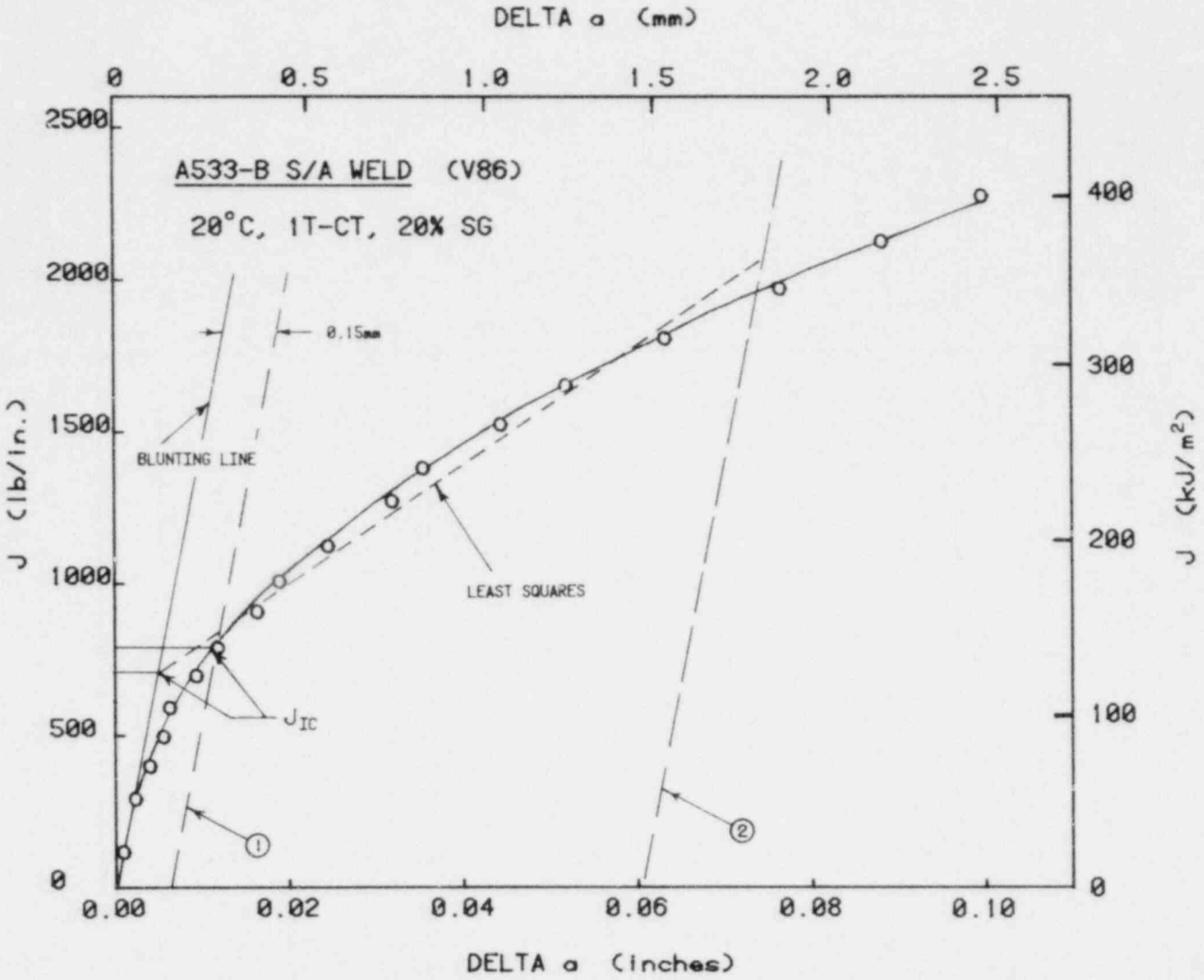

Fig. 14 Illustration of the typical curved behavior of the R curve. An alternative measurement of J_{Ic} is indicated by the intersection of the smoothly drawn R curve with line No. 1 drawn at 0.15 mm crack extension. Also shown is the proposed ASTM definition of J_{Ic}.

believed to be an indicator of the first real crack extension. In other words, any crack extension less than the exclusion line may be difficult to distinguish from blunting. The 0.15 mm exclusion line criterion is also within the projected accuracy of the SSC technique as applied to 1T-CT specimens; however, this accuracy will be more difficult to obtain with larger specimens.

For two reasons an alternative definition of J_{Ic} to that of Reference 10 is proposed here. First, the R curve for nuclear pressure vessel steels appears to exhibit a power law behavior for which a J_{Ic} measurement procedure based upon a least squares fit of the data may be inappropriate. Second, in cases of cleavage failure (Fig. 15) the maximum crack extension can exceed that due to blunting by only a small amount. For this situation insufficient data points may exist so as to preclude a least squares fit. For these reasons an alternative definition of J_{Ic} is proposed: J_{Ic} will be defined here as the J-level corresponding to the intersection of the 0.15 mm exclusion line with a smooth curve through the SSC data points, as illustrated in Fig. 14. A smooth curve through the data is felt to be an accurate representation of the nonlinear characteristic of the R curve. For the case of specimen failure at a crack extension less than that defined by the exclusion line (e.g., some types of cleavage failure) J_{Ic} would be computed at the level of failure.

The advantage of the alternative method for J_{Ic} is that it will define the same value of J_{Ic} irrespective of how little crack extension is developed beyond the exclusion line prior to cleavage failure. Secondly, the method deals with the nonlinear R curve so as not to force a straight line fit to the data points for purposes of J_{Ic} measurement. Note, however, that both the alternative method and the proposed ASTM method can yield comparable values of J_{Ic} for a large crack extension as illustrated in Fig. 14. Thus, it is felt that the two measurement procedures for J_{Ic} are not incompatible.

Figure 15 illustrates the R curve for an A533-B steel specimen which exhibited a small crack extension beyond the 0.15 mm exclusion line before failure in the cleavage mode. This expanded plot highlights the $\pm$0.08 mm ($\pm$3 mil) scatter which can be produced with 1T-CT specimens. (This figure is typical of the largest scatter which has been observed with the current experimental technique). For this case, J_{Ic} is given as 214 kJ/m^2 (1225 lb/in.) by the alternative procedure. Since the crack extension is less than twice the extension to the blunting line, the proposed ASTM procedure would define J_{Ic} at the level of fracture. The latter corresponds to a value of 308 kJ/m^2 (1765 lb/in.) which is 44 percent greater than that given by the alternative definition.

Note that the R curve of Fig. 15 exhibits a sharp change in slope prior to cleavage. This is not a result of data scatter and has been observed with other specimens cut from A533-B steel plate. Possibly this is a new phenomenon associated with a "hardening" of the steel prior to cleavage fracture; this behavior is illustrated by the flattening of the load versus deflection trace just prior to failure (Fig. 10). For a similar-type behavior but at a somewhat greater crack extension, the proposed ASTM procedure requires a least squares fit of the data in order to define J_{Ic}. The hardening phenomenon observed for cleavage failure would appear to make such a least squares fit inappropriate.

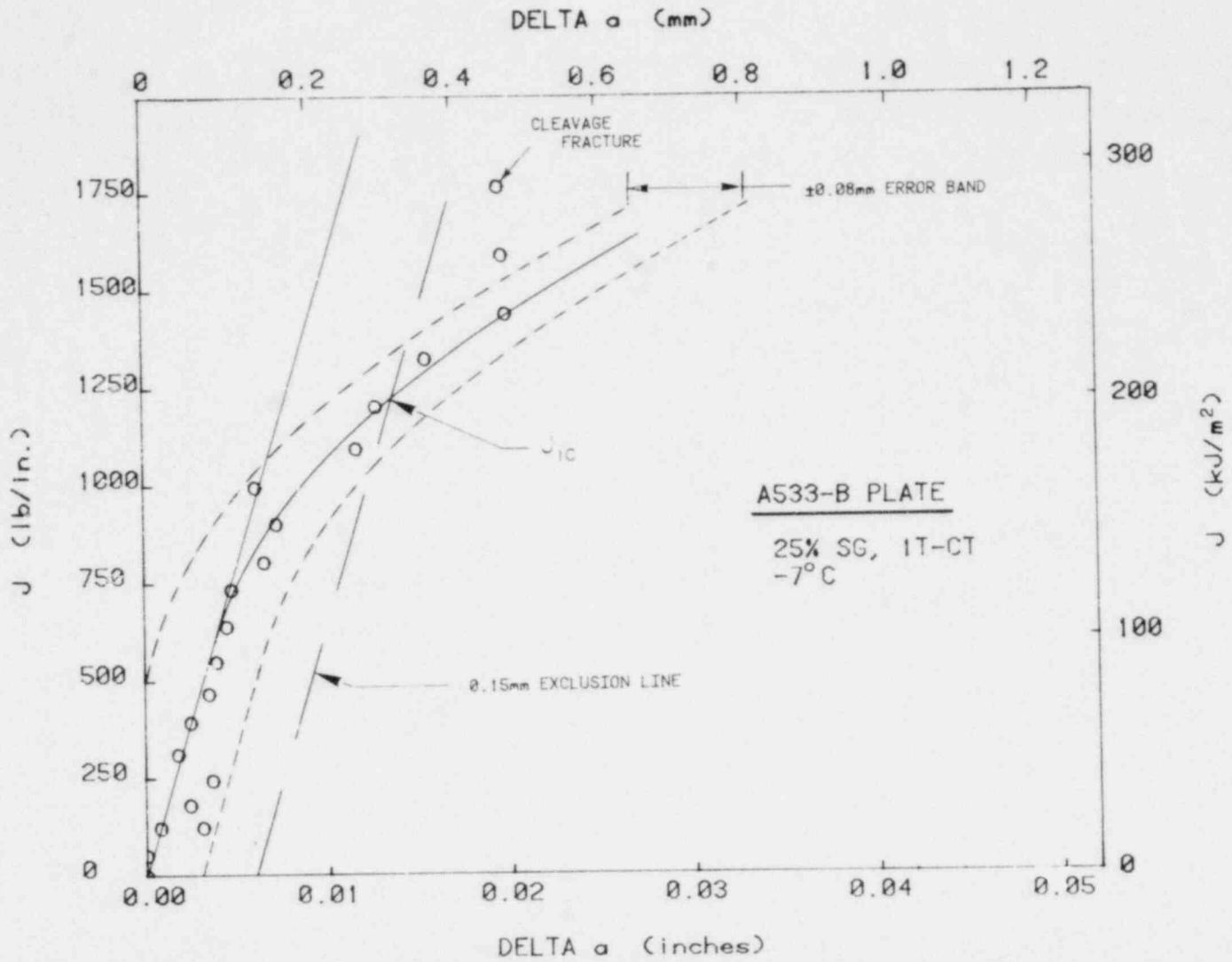

Fig. 15 R curve for an A533-B steel which exhibits a cleavage fracture at a crack extension slightly in excess of the 0.15 mm exclusion line. The scales have been expanded to highlight the data scatter which represents the extremes using current experimental techniques.

Preirradiation CT Specimen Evaluation

Figure 16 illustrates the specimen-to-specimen variability in the R curves exhibited by the submerged arc weld deposit (Code V86). Both specimens were side grooved by 20 percent and tested at different temperatures in the upper shelf temperature region as defined by the C_v test (Fig. 6). These R curves reflect a 36 percent variation in tearing modulus T, from 74 to 106, and a 14 percent variation in J_{Ic}. For purposes of comparison, T is defined here in terms of a least squares fit of the data between the two dashed lines in the figure; this corresponds with the region of crack extension included in the ASTM proposed multispecimen standard for J_{Ic}.

The R curves for specimens having 0 and 10 percent side grooves are compared with preceding data in Fig. 17. Note that 0 and 10 percent side grooves have resulted in identical R curves which lie within the upper scatterband of the specimens having 20 percent side grooves. Figure 18 illustrates the crack front curvature in specimens having 0, 10, and 20 percent side grooves. The specimens with either the 0 or 10 percent side grooves exhibit crack-front tunneling whereas the 20 percent grooves appear to have overcorrected this situation by causing some reverse tunneling. The R curves in Fig. 17 suggest that the specimens with straight crack fronts will exhibit a lesser R curve slope than specimens having a tunneled crack extension.

Figure 19 compares the crack front curvature of a specimen cut from the submerged arc weld deposit (Code V86) with one cut from an A533-B plate. While the 20 percent side grooves have overcorrected the curvature for the weld deposit, this groove depth is insufficient to completely straighten the crack front in the plate material. This comparison suggests that the depth of side grooves required to produce a straight crack front will vary between product forms.

Figure 20 illustrates the toughness variation of the weld deposit as a function of temperature. The plot is presented in terms of K_{Jc}, where this quantity is computed from the relationship:

$$K_{Jc} = \left[\frac{EJ_{Ic}}{1 - \nu^2}\right]^{1/2} \qquad (2)$$

where E and ν are Young's modulus and Poisson's ratio respectively. An upper shelf toughness of 170 MPa $\sqrt{m}$ (155 ksi $\sqrt{in.}$) is indicated for this material. Note that little difference in the K_{Jc} values at a temperature of 200°C is exhibited among specimens having 0, 10 and 20 percent side grooves.

We have chosen to interpret K_{Jc} as the value of K_{Ic} which would have been obtained from a larger specimen meeting the ASTM E-399 size requirements. However, the degree of correspondence between K_{Jc} and K_{Ic} is a topic of research. It should be noted that K_{Jc} can be lower than a K_{Ic} value measured directly. The latter arises from the ASTM definition of K_{Ic} which has a built-in size effect relating to the 2 percent effective crack extension which

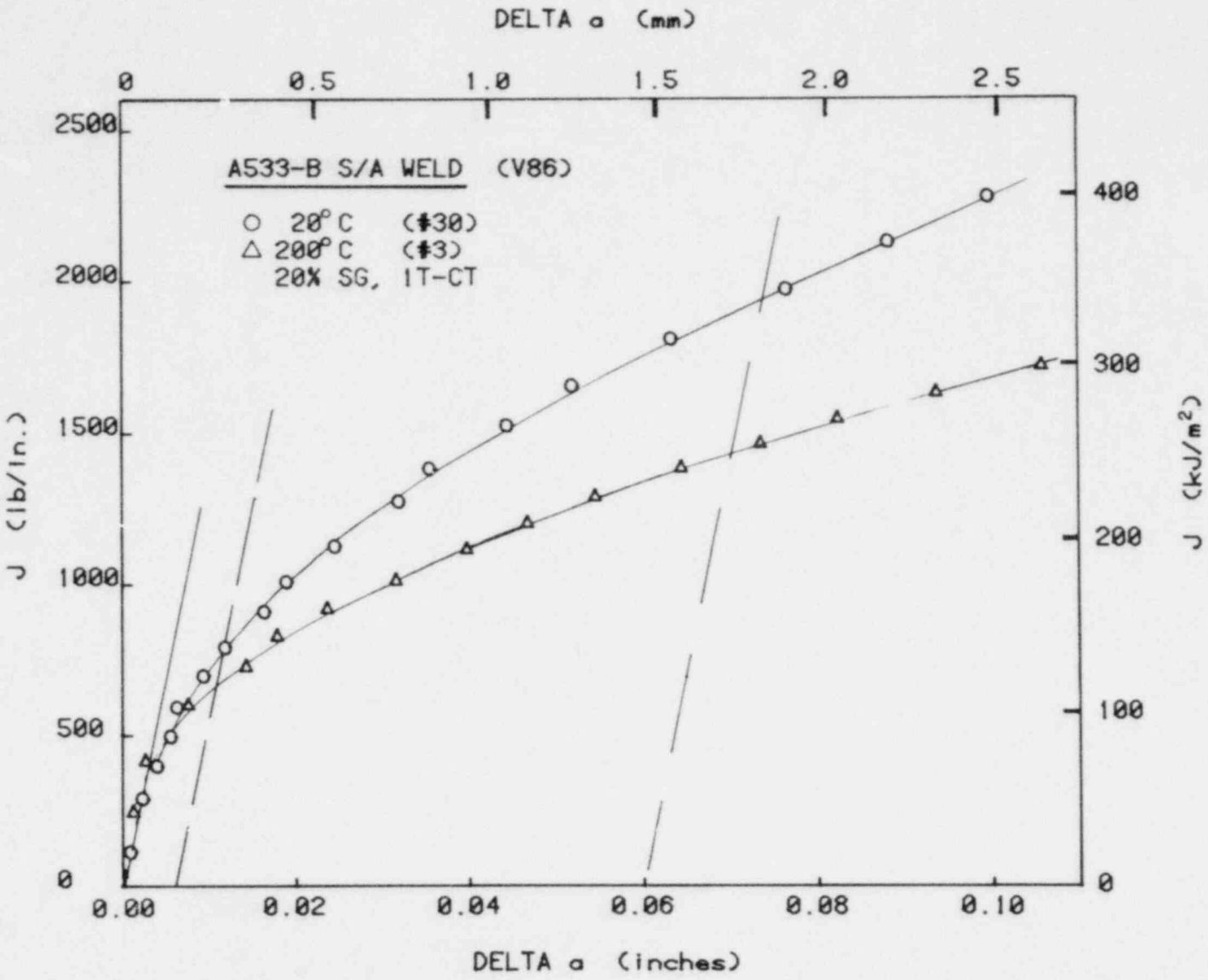

Fig. 16 R curves exhibited by an A533-B submerged arc weld deposit at two temperatures in the upper shelf regime.

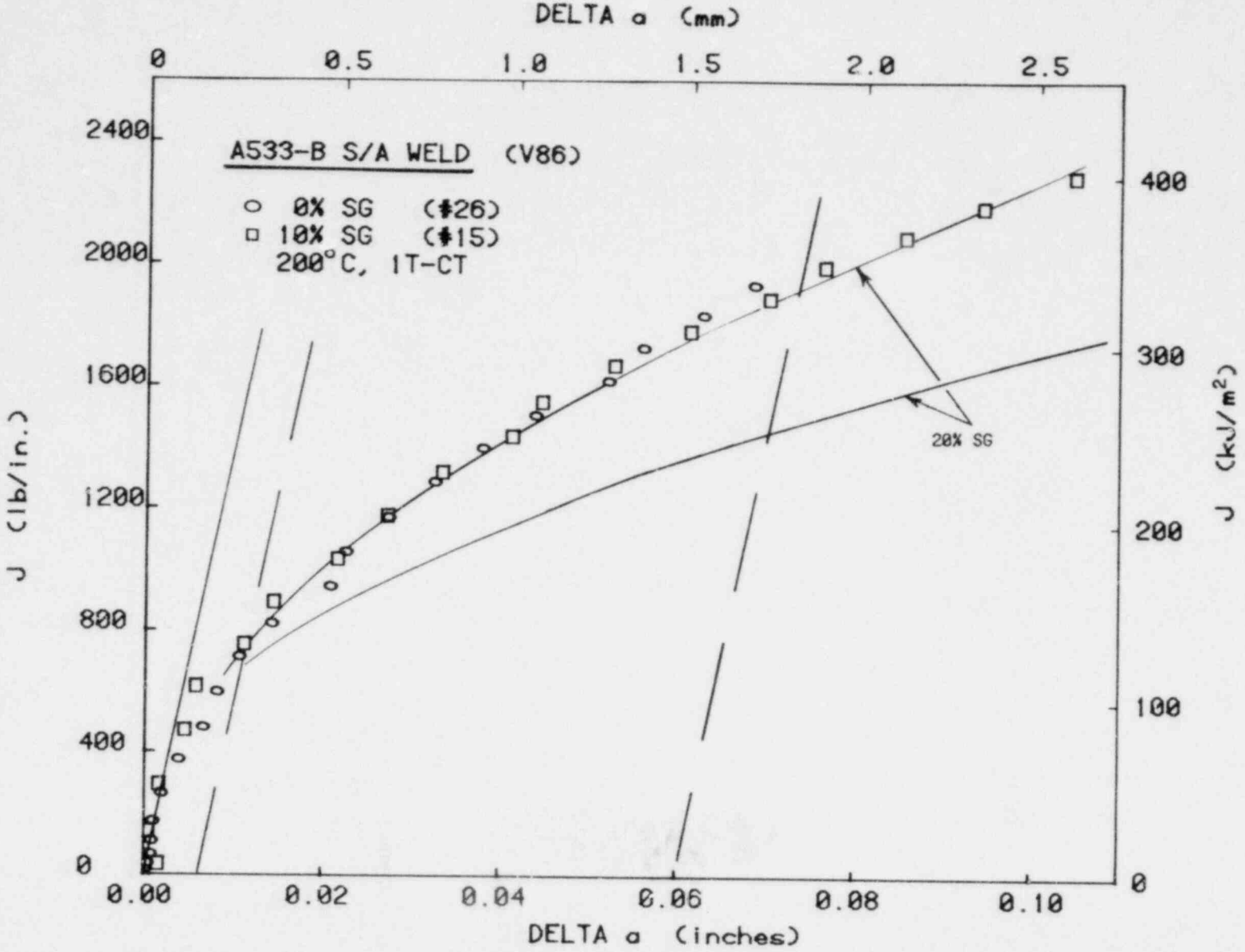

Fig. 17 R curves for specimens having 0 and 10% side grooves are compared with the trend defined by specimens having 20% side grooves (Fig. 16).

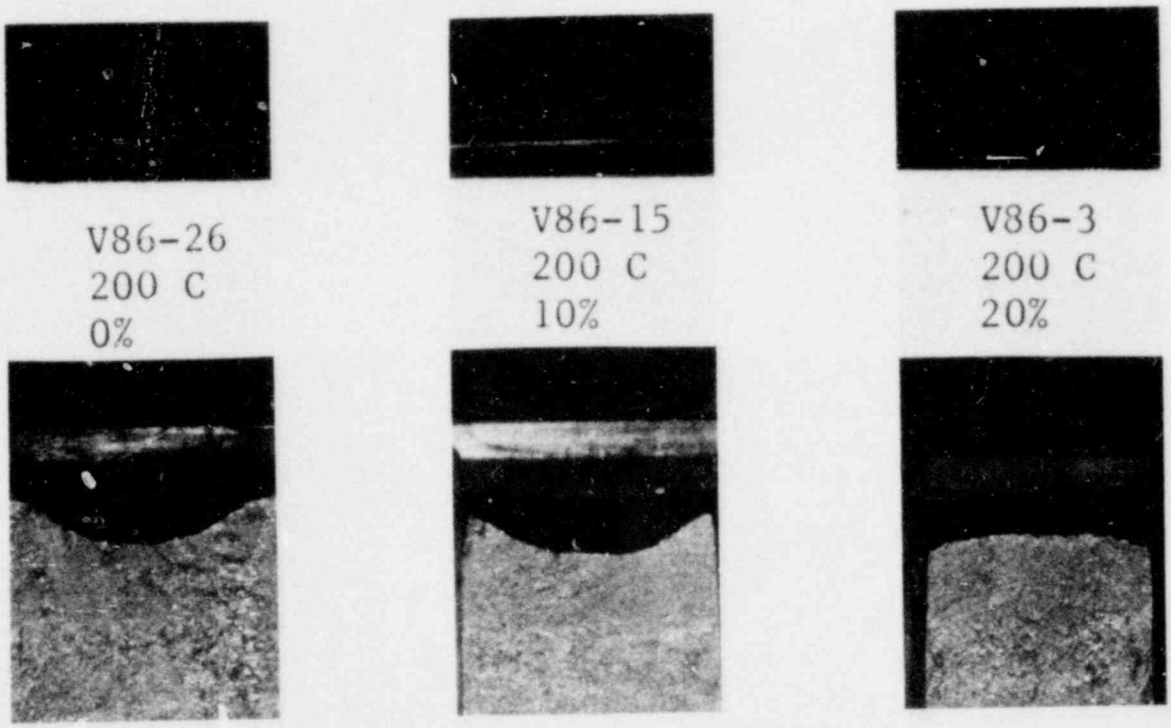

Fig. 18 The influence of 0, 10 and 20% side grooves (left to right) on crack-front shape. No apparent difference in crack-front shape exists between the specimens having 0 and 10% side grooves. However, a slight overcorrection has occurred as illustrated by the reverse tunneling exhibited by the specimen with 20% side grooves.

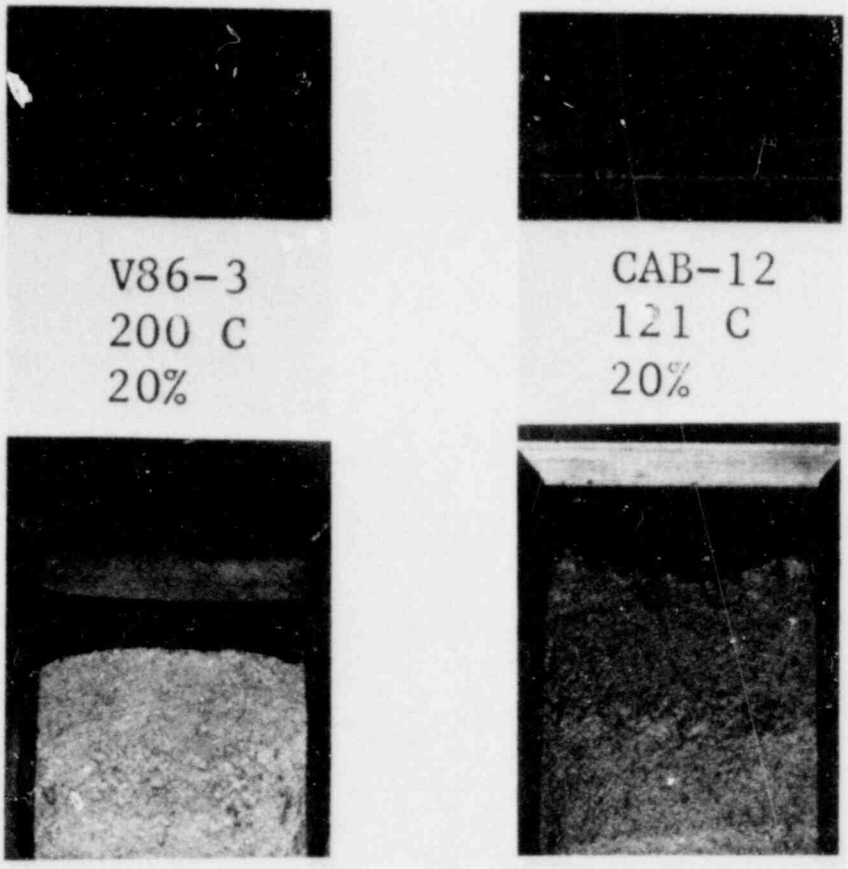

Fig. 19 The variable effect of 20% side grooves on crack front shape is illustrated for 1T-CT specimens cut from A533-B submerged arc weld deposit (left) and A533-B steel plate (right). The influence of side grooves in straightening the crack front appears to be alloy dependent.

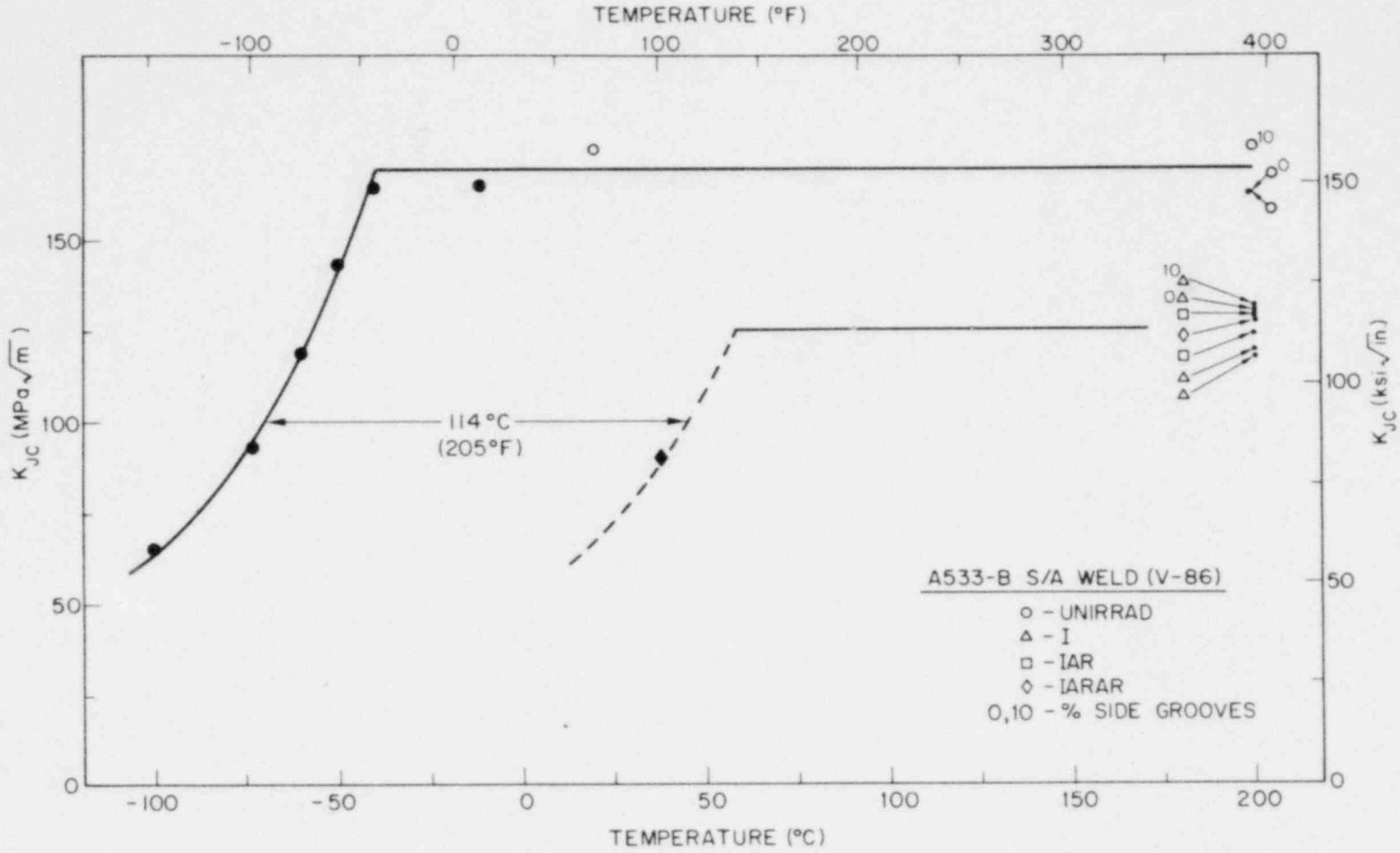

Fig. 20 Comparison of pre- and postirradiation fracture toughness (K_{Jc}) as computed from Eq. 2. The temperature elevation of the toughness for the irradiated material, as projected from the C_v 41J energy level, is indicated by the dashed lines. The filled symbols denote cleavage fracture preceded by some ductile crack extension; the open points denote ductile crack extension without cleavage. All tests had 20% side grooves except as noted.

is permitted in E-399. Clearly, crack extensions of this magnitude in large-size specimens could result in K_{Jc} values considerably in excess of a K_{Jc} level based on a fixed crack extension beyond the blunting line such as 0.15 mm.

CT Specimen Evaluation of Irradiated Weld Depsoit

Irradiated specimens of the weld deposit (Code V86) have been investigated in the I, IAR and IARAR conditions. The fluences and annealing conditions are identical to those of the C_v specimens described in the preceding section. The majority of the tests have been conducted at a temperature of 200°C (392°F) which corresponds to the C_v upper shelf regime for both the irradiated and unirradiated material (Fig. 6). The results of all tests are listed in Table 6.

Figure 21 compares the J-R curves of the unirradiated material (Fig. 16) with those from two irradiated specimens in the I condition. Both irradiated tests define a J_{Ic} value of 65 kJ/m^2 (373 lb/in.) which is half of the unirradiated value. The corresponding K_{Jc} of the irradiated material is 119 MPa $\sqrt{m}$ (108 ksi $\sqrt{in.}$). The tearing modulus of the irradiated tests in Fig. 21 is approximately 30 as defined by a least squares fit through the data as previously discussed. This value of T is only one-third of the average value shown by the unirradiated material having 20 percent side grooves. Since the R curve exhibits a nonlinear behavior, the value of T decreases with crack extension. For example, at a crack extension corresponding to the dashed line (No. 1), the value of T is approximately 18.

A comparison has been made of the crack-front curvature exhibited by irradiated specimens (I condition) having 0, 10, and 20 percent side grooves. (The corresponding R curves are shown in Fig. 22.) As contrasted to the unirradiated case, the specimen with 10 percent side grooves exhibited a straight crack front as did the specimen having 20 percent side grooves. Thus it appears that the increased flow stress of the irradiated material may have permitted the use of a smaller percentage side grooves. Unfortunately, this conclusion cannot be generalized in that 10 percent side grooves resulted in a deeply tunneled crack front in an irradiated A533-B specimen tested in another program. However, 20 to 25 percent side grooves have produced a straight crack front in all cases thus far.

In Fig. 22, the R curve for the specimen without side grooves is above the data band formed by the specimens having 10 and 20 percent side grooves. This behavior is consistent with that of the unirradiated tests (Fig. 17) and suggests that the R-curve slope is proportional to the degree of crack-front tunneling; a lower bound R curve appears to be exhibited by specimens having a straight crack front even though various side-groove depths were employed to achieve this behavior.

The J-R curve trends from IAR and IARAR specimens tested in the upper shelf temperature regime are illustrated in Fig. 23. The results show that J_{Ic} of the reirradiated material is the same or slightly better than that of the I condition. On balance the R curves of the IAR and IARAR specimens are also slightly higher than those of the I-condition specimens. These results are

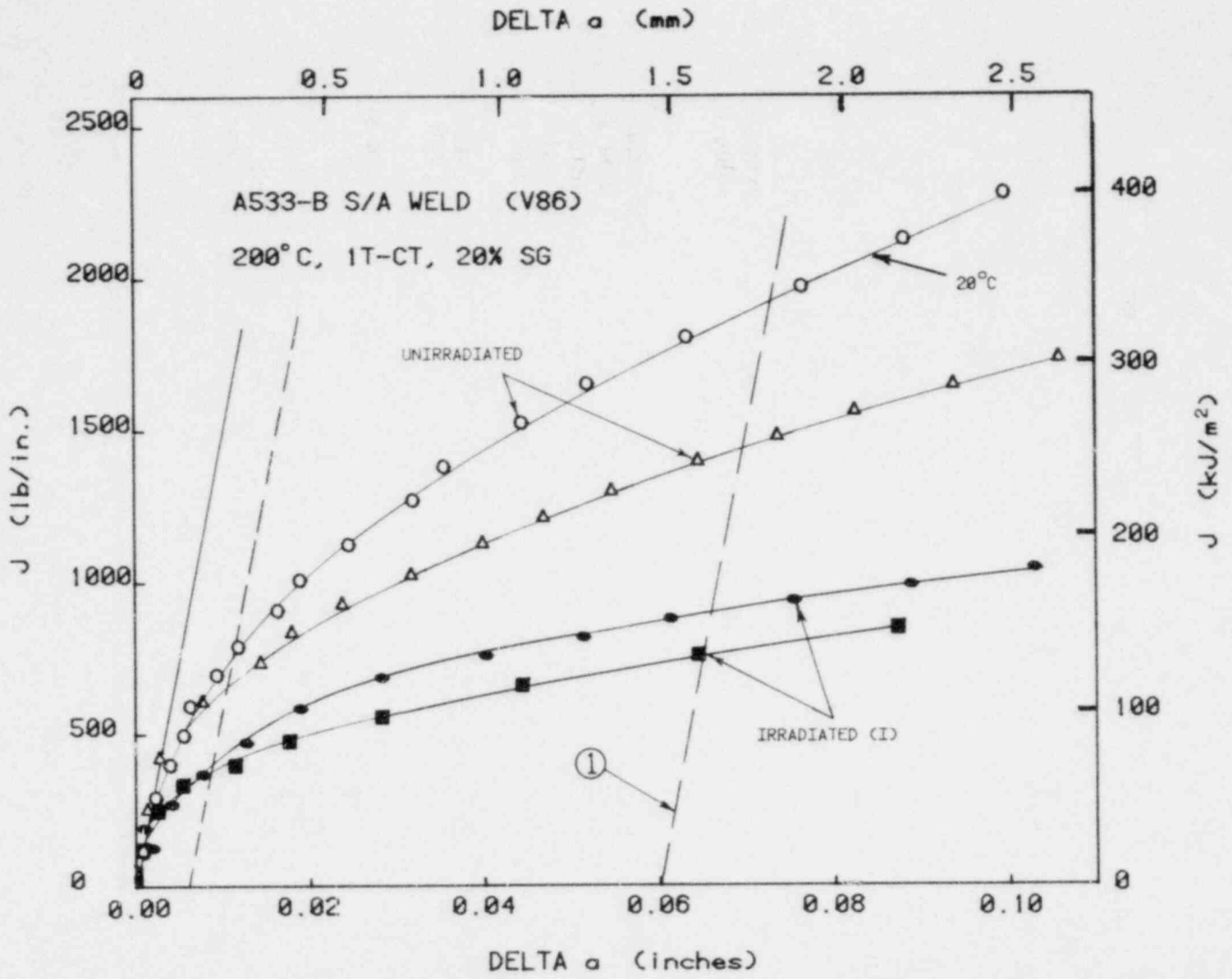

Fig. 21 R curves for irradiated weld deposit (I condition) are compared with those for the unirradiated condition (Fig. 16). The postirradiation J_{Ic} and T values are one-half and one-third of those for the unirradiated condition, respectively.

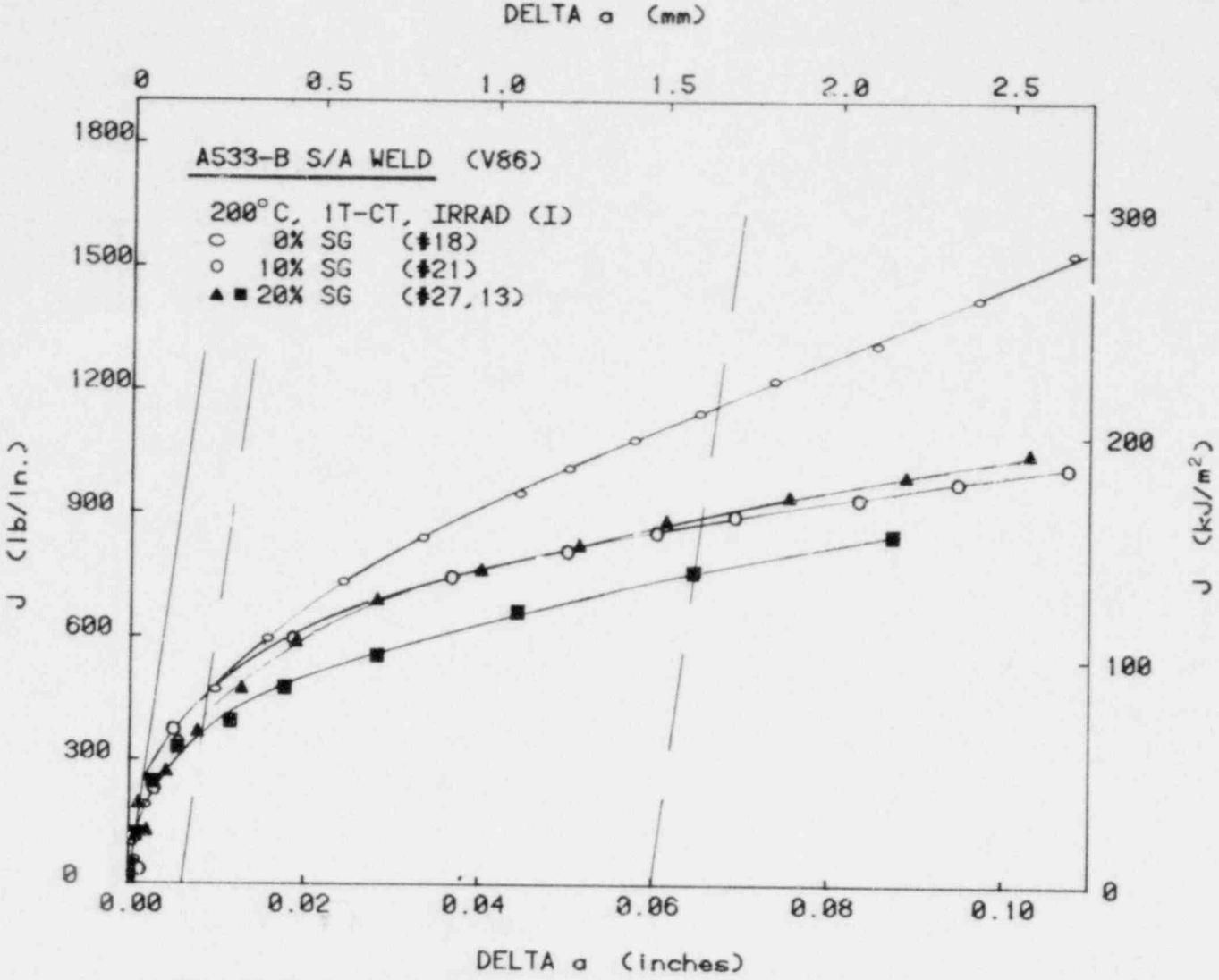

Fig. 22 Comparison of R curves for irradiated specimens (I condition) having 0, 10 and 20% side grooves.

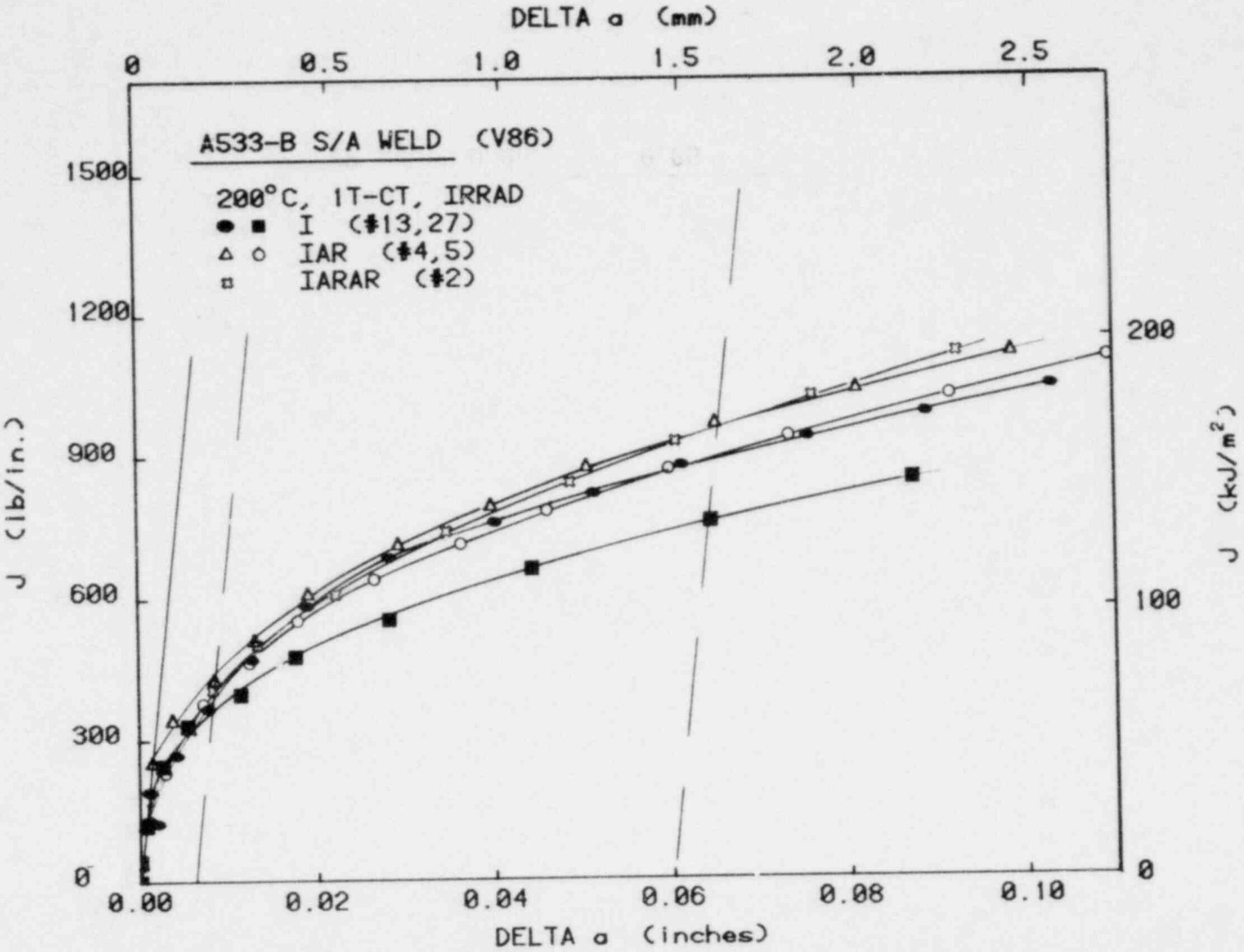

Fig. 23 Comparison of R curves for irradiated weld deposit (I) with those for material which has been reirradiated with intermediate annealing (IAR, IARAR).

consistent with the small improvement in C_v upper shelf energy previously illustrated for these irradiation conditions (Figs. 6 and 8).

In terms of K_{Jc}, Fig. 20 compares the toughness of specimens in the I, IAR and IARAR conditions. For the specimen with 20 percent side grooves, the toughness in the IAR and IARAR conditions shows a slight improvement over that defined by the I condition. On balance, however, little variation is shown between the irradiated and reirradiated conditions. These results are consistent with those of the C_v tests. Therefore, it is concluded that annealing has been successful in mitigating the embrittlement which would have resulted in a material having accumulated a total fluence of the IAR and IARAR condition without the benefit of intermediate anneals.

A single specimen from the IARAR condition has been tested to a temperature within the transition region. As expected, the R curve for this specimen exhibited very little crack extension prior to cleavage failure and J_{Ic} was taken as the value at failure. This result, plotted in Fig. 20, is to be compared with the estimated trend for irradiated material (dashed curve). The latter was obtained by elevating the transition curve for the unirradiated material by a temperature increment equivalent to the shift in the C_v curves at the 41J energy level (Fig. 8). It can be seen that the position of the experimental result in Fig. 23 is consistent with that projected from the C_v trends.

III. FATIGUE CRACK PROPAGATION IN LWR MATERIALS

A. Evaluation of Critical Factors in Cyclic Crack Growth Rate Studies

W.H. Cullen, Jr., H.E. Watson, K. Torronen,[1] V. Provenzano, F.J. Loss, and G. Gabetta[2]

Background

For the past two years, the cyclic crack growth rate program at NRL has followed a preliminary matrix test plan prepared by NRC and NRL. The plan was designed to evaluate, for a single material (A508 steel), the effect of ramp time (1 sec-30 min) hold time (1 min-60 min) and temperature (93 and 288°C) on crack growth rate, with the objective of determining the most aggressive test conditions for subsequent tests. These tests, carried out at a load ratio of 0.2 and in pressurized, deoxygenated reactor grade water [1000 ppm boron, 1 ppm lithium, i.e., presurized water reactor (PWR) conditions], were designed to simulate heatup, cooldown, and hydro-leak-test conditions. This period was also used to develop and improve test facilities as well as to refine methods of data acquisition and reduction. This effort has been coordinated with the Westinghouse Nuclear Power Systems Division [11-17].

In December 1978 it was determined that the objectives of the preliminary matrix had been met. Building on these results, the main matrix has been developed which includes a variety of pressure vessel materials including plate, forging, and weld/flux combinations. As with the preliminary matrix, these testing responsibilities will be shared with Westinghouse. The administration of the program will be carried out by NRL. Table 7 indicates the materials, waveforms and load ratios selected as elements of this test plan. Load ratios of 0.2 and 0.7 have been chosen for the initial tests in order to yield data at these extremes; tests at the intermediate value of 0.5 will follow if necessary. A program of tests on irradiated steels will also be carried out as part of the main matrix. The elements of this test plan are listed in Table 8. Additionally, NRL has assumed responsibility for evaluation of the effect of the main matrix test parameters on a variety of piping materials including welds. This program was initiated in March 1979.

Preliminary Matrix Results

The results of tests selected from the preliminary matrix plan, together with supporting tests, are shown in Figs. 24-27. Figures 24 through 26 are paired according to certain characteristics of the waveforms and the lower temperature (93°C) results are on the left and the higher temperature (288°C) results are on the right. There are three factors which strongly influence the crack growth rate in A508-2 in the reactor grade water environment; these are the prime variables of the preliminary matrix scheme: rise time, hold time and temperature. An interrelationship among the three determines the particular crack growth rate; it is impossible to isolate one variable without fixing the other two.

Permanent addresses:

[1]Technical Research Centre of Finland, 02150 ESPOO 15, Finland

[2]CISE, Via Reggio Emilia, Segrate (Milano), Italy.

Table 7 Main Test Matrix (Unirradiated Materials)

	R = 0.2		R = 0.5		R = 0.7	
	1 cpm Sinewave	1 min Ramp	1 cpm Sinewave	1 min Ramp	1 cpm Sinewave	1 min Ramp
A508	4C+S	2C+S	D	D	1C+S	S+U
Linde 80	2S	2S	D	D	2S	2S
Linde 80 - HAZ	2S	2S	D	D	2S	2S
Linde 0091	2S	2S	D	D	2S	S+U
Linde 0091 - HAZ	S	2S	D	D	2S	2S
Linde 124	S+U	2S	D	D	2S	2S
Linde 124 - HAZ	D	S	D	D	D	S
A533-B	2S	2S	D	D	2S	S+U

Entries reflect combined Westinghouse and NRL effort.
S - Test scheduled
C - Test completed
D - Test deferred
U - Test underway

Table 8 Main Test Matrix (Irradiated Materials)

	R = 0.2		R = 0.5		R = 0.7	
	1 cpm Sinewave	1 min Ramp	1 cpm Sinewave	1 min Ramp	1 cpm Sinewave	1 min Ramp
A508	S	S	D	D	S	S
Linde 80	2T	2T	D	D	2T	2T
Linde 80 - HAZ						
Linde 0091	2S	S	D	D	S+T	S+T
Linde 0091 - HAZ						
Linde 124	2S					
Linde 124 - HAZ	S					
A533-B	2S	S	D	D		2T

Entries reflect combined Westinghouse and NRL effort.
Blank - No test or irradiation scheduled at present
S - Test scheduled
T - Test tentative, pending other test results
D - Test deferred

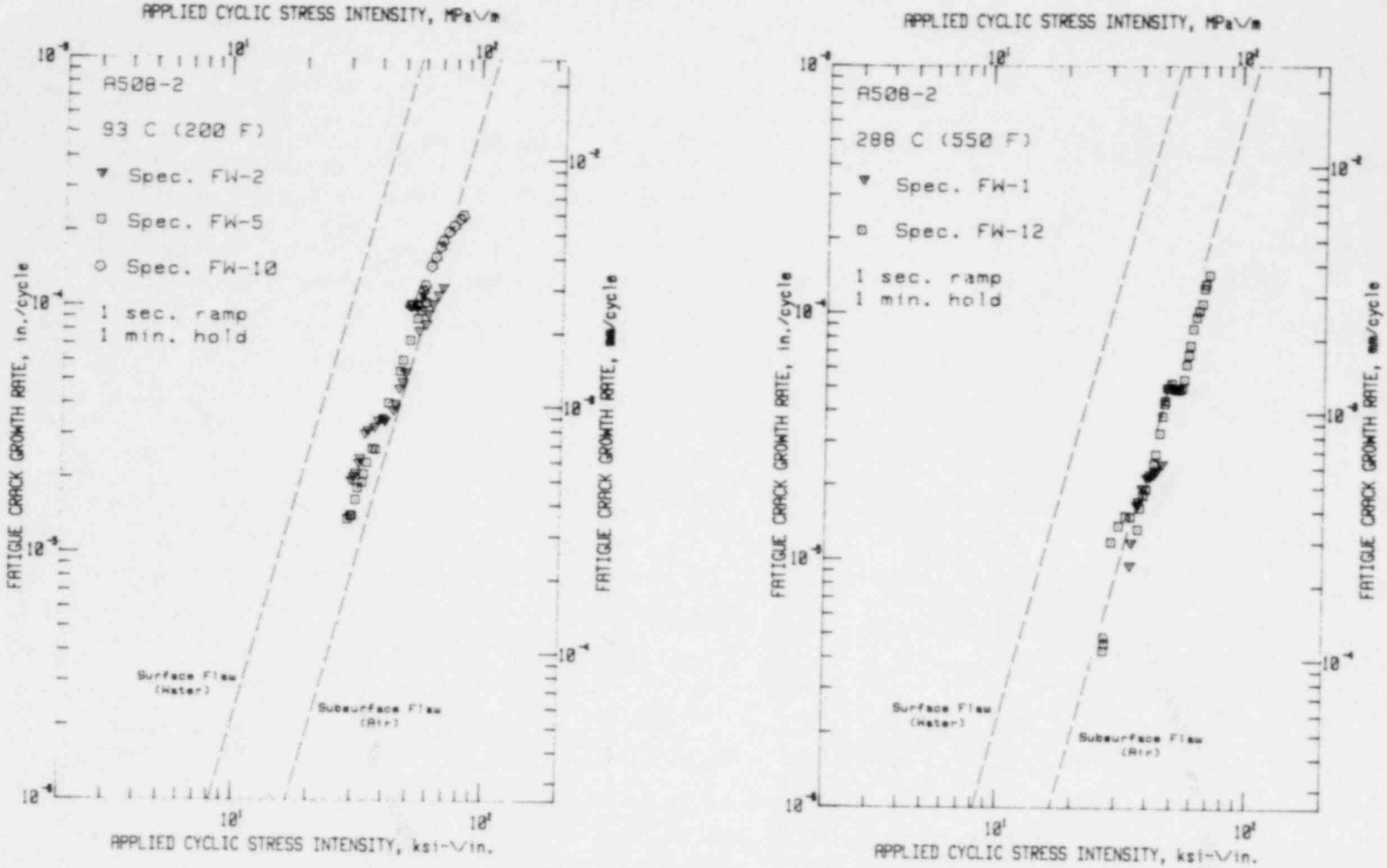

Fig. 24 Fatigue crack growth rate data vs applied cyclic stress intensity for all the tests with a very short (1 sec) rise time. In this and the two following figures, the lower temperature test results are on the left. Both these temperatures yield growth rates close the ASME Section XI air default line. It is believed that this ramp time is too fast to allow significant hydrogen admission and the crack growth rate is thus unassisted by any hydrogen mechanism.

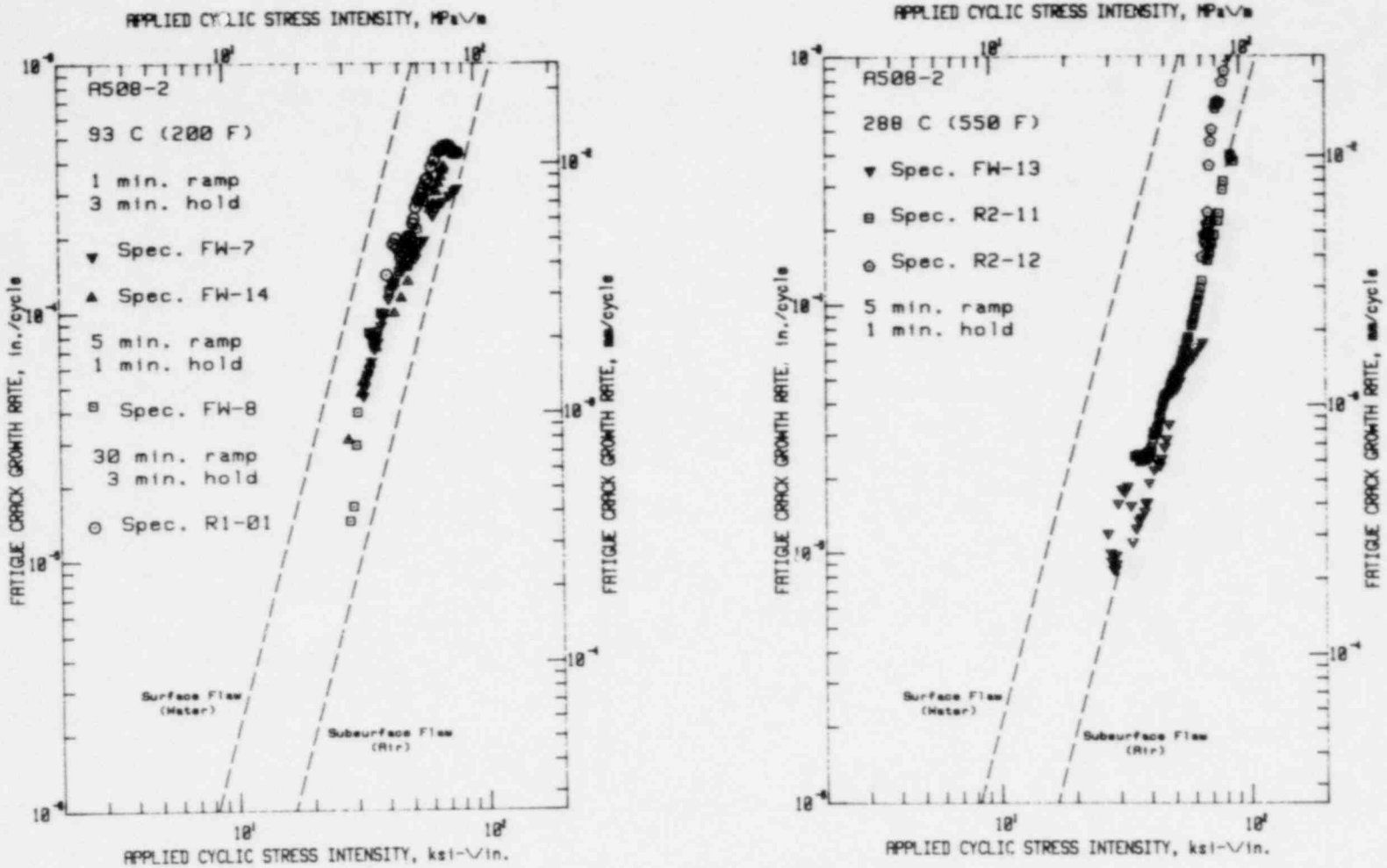

Fig. 25 Fatigue crack growth rate data vs applied cyclic stress intensity for all the tests with both significant ramp times and hold times (1 min or greater for each). In the left hand data sets, the effect of the increased growth rates due to the lower temperature is clearly seen. In this case, the test at low temperature shows the effects of hydrogen assistance, and the resultant fracture surfaces bear the characteristics of this mechanism. The higher temperature tests do not exhibit high growth rates, possibly because the formation of an oxide layer prevented significant hydrogen entry.

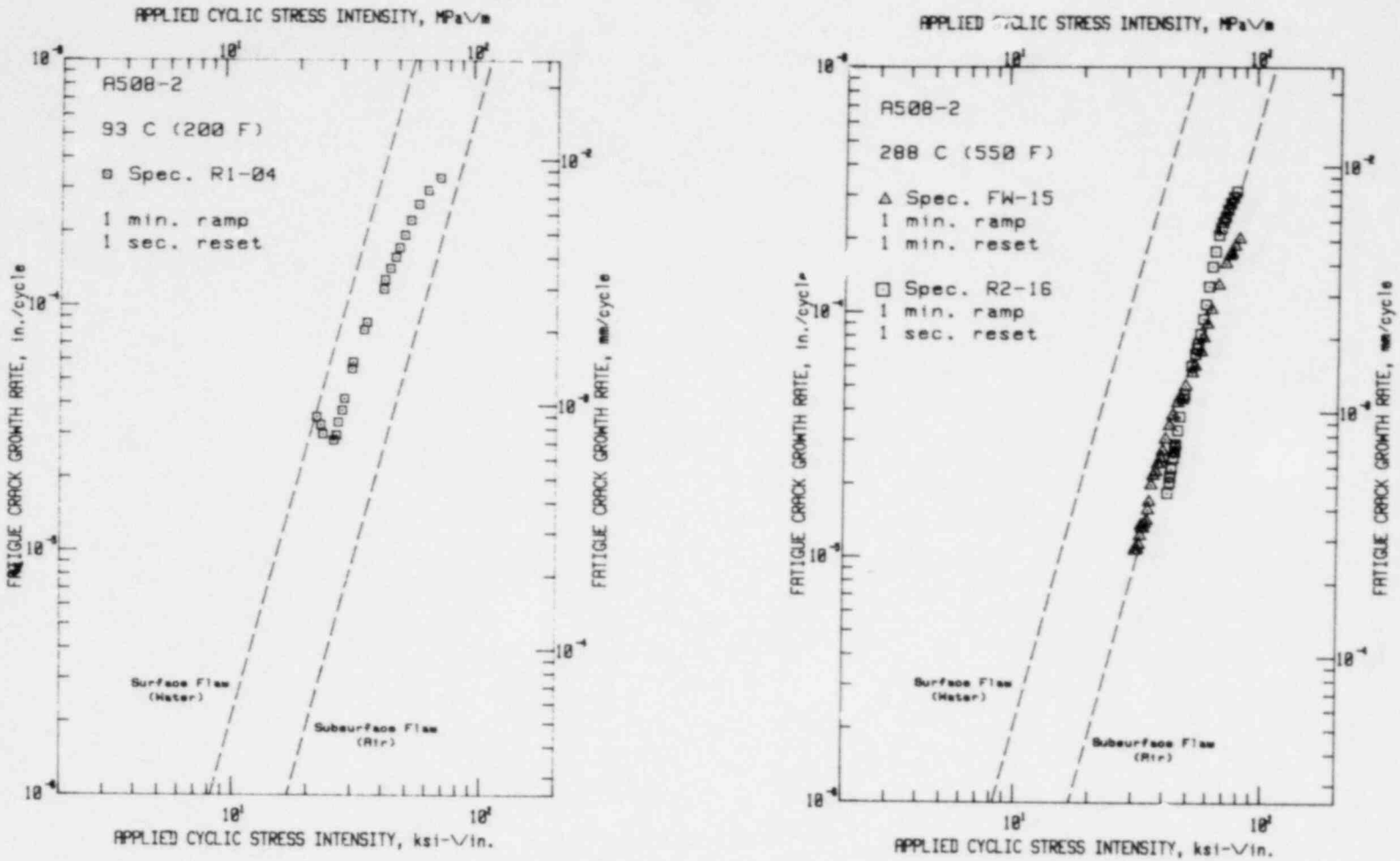

Fig. 26 Fatigue crack growth rate data vs applied cyclic stress intensity for tests with a one min ramp, but no hold time. The fact that the low temperature test exhibits a high growth rate, and the high temperature test does not, is an indication of either the difference in the permeability of the oxide layer, or of the temperature dependence of the mobility of interstitial hydrogen.

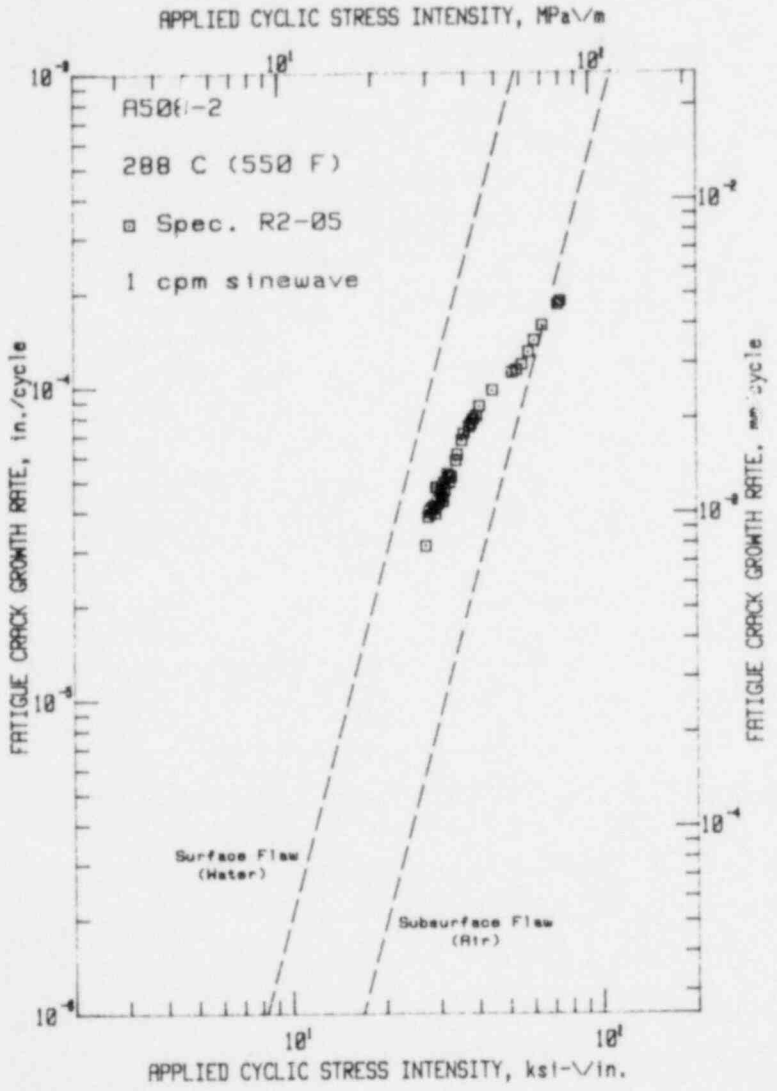

Fig. 27 Fatigue crack growth rate data vs applied cyclic stress intensity for a test with a 17 mHz (1 cpm) sine waveform. These data, the only test to exhibit a high growth rate at a high temperature, suggest that there is a ramp time of approximately 30 sec during which the hydrogen can gain entry and result in increased crack growth rates.

An examination of all the data sets produced under the guidelines of the preliminary matrix, together with other tests run under similar environmental conditions but utilizing non-matrix waveforms, indicates that each data set falls into one of two rather clearly defined categories. One band of data lies close to, or essentially on, the ASME Section XI Code air environment default line. This class of data, exhibiting the lower of the two crack growth rates, will be called "low." The other band of data, which resides a factor of three to five above the first, will be termed "high." This latter band of data resides approximately midway between the Section XI air and water environment default lines.

Figure 24, showing data from tests with a fast (1 sec) ramp time, and Fig. 25, showing data from tests with a longer ($\geq$1 min) ramp time indicate that combinations of long ramp times and low temperature (93°C) result in growth rates belonging in the "high" category. Regarding the high temperature (288°C), it is impossible to determine, from Figs. 24 and 25, whether the longer ramp, or the hold time are solely responsible for the low crack growth rate results. Figure 26 shows the results of tests involving 1 min ramp times, and no hold time, and the results for high temperature are in the low category. Thus, it is clear that a hold time is not required to produce low growth rate data at the higher temperature. On the other hand, at the lower temperature, a ramp time component is sufficient to produce a high growth rate, and comparison with Fig. 12 shows that a hold time component does not additionally aggravate the growth rate. Lastly, Fig. 27 shows the results of a 17 mHz (1 cpm) sinewave test which produced data in the high growth rate category. If the sine waveform is interpreted as an increasing ramp of approximately 30 sec duration, then this implies that there is a maximum crack growth rate dependence on ramp time which lies between 1 and 60 sec; a ramp time of 30 sec yields a higher crack growth rate than ramp times of 1 or 60 sec.

At the close of this quarterly reporting period, confirmation of this behavior was being sought through a series of additional tests involving ramp times of about 20 to 30 sec, with and without hold times. The fact that 17 mHz sine waveforms yield high growth rate data is incontrovertible, and the realization of these same crack growth rates for a linear ramp test is possible by simply choosing the appropriate ramp rate.

A primary objective of the prliminary matrix was to determine if any conditions could be found which would produce data which exceeded the ASME Section XI water default line. A very limited amount of data had been previously published [4] showing that a 17 mHz sinewave and a load ratio of 0.2 would just marginally exceed this limit, but a much larger amount of data for R = 0.6 [8] and 0.7 [4] shows that the limit would be exceeded over a significant range of cyclic stress intensity. However, consideration of the NRL preliminary matrix data indicates that the ASME Section XI water default line is not exceeded for these load ratios (0.2), temperature (93, 288°C), and waveform (ramp/hold, sinewave) conditions.

Hydrogen Assisted Crack Growth Model and Fractographic Results

As these results have begun to cohere, a model for hydrogen assisted crack growth has evolved to help understand and interpret these results. As

with most models for hydrogen embrittlement in aqueous media, hydrogen is generated by a cathodic reaction at the crack tip. This occurs only during rise time of the fatigue cycles as fresh metal surface at the crack tip is exposed. Hydrogen generated during this hydrolysis can enter the metal and diffuse to the region of high triaxial strain just ahead of the crack tip, producing a local embrittlement and resulting in an accelerated crack growth rate. However, this effect may be countered by other considerations. For example, anodic dissolution may induce an increase in crack growth rate [19], or it can create the opposite effect, namely, blunting and crack growth retardation [20-22]. At higher temperatures, the formation of a stable oxide inhibits entry of hydrogen at the crack tip provided that the ramp time is long enough to allow this [22]. On the other hand, a very short ramp time allows neither the hydrogen entry, nor the oxide formation, and hydrogen-assisted growth is not expected.

With some refinements, the above model can be employed to understand the crack growth behavior observed. For the fast ramp time tests, growth rates are low because the hydrogen cannot be evolved, absorbed and admitted to the matrix in the quantities necessary for measurable assistance to the crack growth rates. For the longer ramp times, and at the lower temperatures, the hydrogen can be formed at the crack tip and can diffuse into the plastic enclave. The temperature is low enough that an oxide layer either cannot be formed fast enough, or the layer, if formed, is porous enough to allow hydrogen admission. The mobility of hydrogen is low enough that it is retained in the plastic enclave rather than diffusing on into the bulk.

At the higher temperature, it is again probable that the fast ramp times do not permit the hydrolytic reaction to occur to any large extent. For the longer ramp times, the resultant low growth rate data leads to the conclusion that here also there is little or no hydrogen assistance. It is possible that 1 min ramp times are sufficient to allow formation of a passivating oxide layer, or that stress relaxation processes at the crack tip result in blunting and resultant retardation of crack growth rates.

The 17 mHz sinewave data, which exhibits a high crack growth rate, suggests that there is some sub-range of ramp times, between 1 sec and 1 min, which produce high crack growth rates. Mechanistically, this might be explained as the time range which is sufficient to allow hydrogen entry to the metal, but insufficient to allow passivation or blunting. At the end of this reporting period, an additional test, with a 22 sec ramp time, was being run to help determine the waveform resulting in the highest crack growth rates.

The details of this model are well supported by the fractographic observations of the fatigue fracture surfaces. The influence of hydrogen assistance on the fatigue crack growth rates often manifests itself on the fatigue fracture surface in several ways including added cleavage or quasi-cleavage, a greater percentage of intergranular failure and a lesser percentage of fatigue striation formation. Many of the specimens from the preliminary matrix test series have been examined both metallographically and fractographically, and the results of these observations are given in Table 9.

Table 9 Summary of Fatigue Fracture Surface Characters as Functions of Temperature, Rise Time and Hold Time

Table 3a Tests With Long Hold Times

	Short Rise Time	Long Rise Time
Low Temp	Transgranular ductile failure, fatigue striations, secondary cracking.	Mostly transgranular failure with quasi-cleavage facets, some intergranular failure. Absence of fatigue striations, fewer secondary cracks.
High Temp	Transgranular ductile failure, fatigue striations, secondary cracking.	Transgranular ductile failure, fatigue striations, secondary cracking.

Table 3b Tests With No Hold Time

	Short Rise Time	Intermediate Rise Time	Long Rise Time
Low Temp	N.A.	N.A.	Mostly transgranular failure with quasi-cleavage facets, some intergranular failure. Absence of fatigue striations, fewer secondary cracks.
High Temp	N.A.	Transgranular failure with fatigue striations, some cleavage-like facets, fewer secondary cracks.	Fractographic examination underway

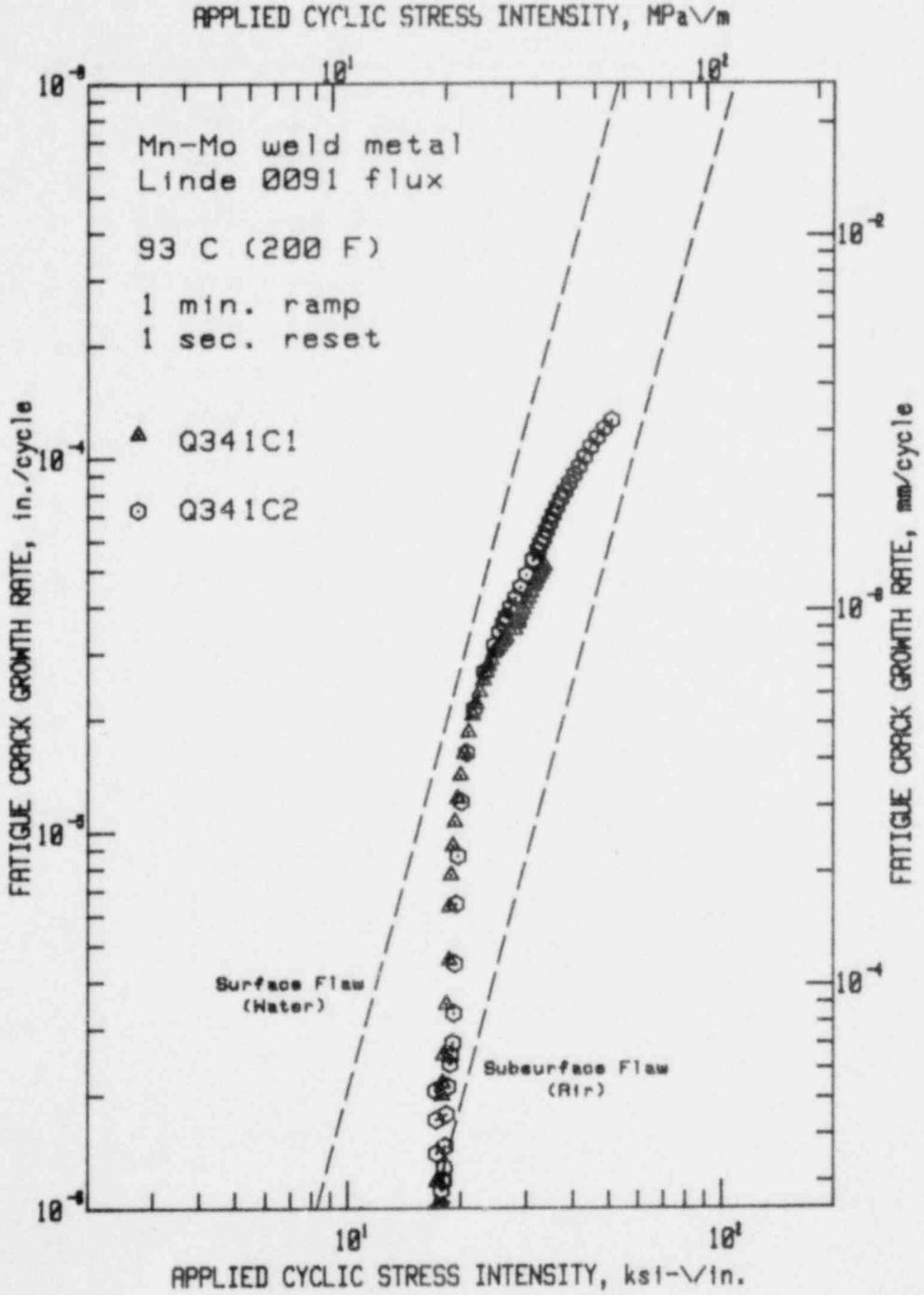

Fig. 28 Fatigue crack growth rate data vs applied cyclic stress intensity for two specimens of Mn-Mo weld metal in PWR reactor-grade water at 93°C. These data compare with the data in Fig. 3a, showing that the growth rate is in the high category for this long ramp time and low temperature set of conditions.

Progress on Main and Piping Test Matrices

As indicated in Table 7, several main matrix tests of A508 steel have been completed although at the time these tests were conducted in support of the preliminary test matrix plan. Preparation of specimens and several other tests, of both main matrix and piping steel materials, are underway. The materials currently under test include A533-B steel plate, A508 steel forging, Mn-Mo weld metal (Linde 0091 flux), and A106 piping steel. These materials are being tested under simulated PWR conditions at 288°C using a load ratio of 0.7 and a 1 min ramp/reset (positive sawtooth) waveform. In addition to the A106 piping steel test included above, several other piping steel tests are planned. These include A516 steel and specimens cut from a large stainless and carbon steel research vessel.

Data from low temperature tests of main matrix material (Q34 - Mn-Mo weld Linde 0091 flux) is shown (93°C) in Fig. 28. These data show the expected high growth rate from a one min ramp/reset waveform at low temperature as discussed above. The fracture surfaces will be examined in order to better determine the exact reasons for this crack growth rate behavior.

Preparation for Initiation of Irradiated Corrosion Fatigue Tests

Two single specimen autoclaves will be utilized for the unirradiated specimen tests. One of these autoclaves, capable of testing a 1T-CT specimen, is installed in the hot cell. So far, this facility has been devoted to preliminary matrix testing. Preparations are now being made to conduct the first test of an irradiated specimen. Fourteen irradiated 1T compact specimens are available for testing in this autoclave.

The second autoclave chamber has the capacity for 2T or 4T CT or WOL specimens. This chamber will be installed in a hot cell within the next two months. A total of four 2T CT specimens have been irradiated and are currently available for testing in this autoclave. Both the 1T and 2T specimens irradiated for the hot cell autoclave tests were machined from either A508 forging, A533 plate, or Linde 0091 weld materials.

B. Fractographic and Microstructural Investigation of Fatigue Specimens of A302 Grade B Steel

G. Gabetta[1] and V. Provenzano

Background

The studies of fatigue crack propagation (FCP) behavior of ferritic steels for pressure vessel applications are of primary importance to light water reactor safety. One of the many objectives of current FCP studies is to test the validity of ASME Code Section XI curve for materials in nuclear environments. Further, these studies are aimed at understanding the complex mechanisms of fatigue failure as a function of the significant fatigue variables which include material condition and environment.

[1]Permanent Address: CISE, Via Reggio Emilia, Segrate (Milano), Italy.

The light water reactor safety programs involving the ferritic steels are of interest to many countries. In Italy, a research program in this field is sponsored by the Italian Electric Power Company (ENEL) and is being carried out at the Centro Informazioni Studi Esperienze (CISE) research laboratory in Milan, Italy. In support of the CISE research program for ENEL, preliminary FCP tests in air at room temperature were conducted on low shelf A302-B steel procured by the Naval Research Laboratory (NRL) to characterize early production of nuclear pressure vessels. These studies on A302-B steel are part of a cooperative research program between NRL and CISE to investigate the fatigue and fracture properties of ferritic steels for nuclear pressure vessel applications. This cooperative program is sanctioned and encouraged by the U.S. Nuclear Regulatory Commission (NRC).

Since the rolling procedure used in steelmaking is known to effect the microstructure of ferritic steels [23], preliminary tests were designed to investigate the effect of rolling direction on FCP behavior of A302-B ferritic steel. The FCP tests included in the present study were carried out at the CISE laboratory; the fractography and x-ray microanalysis on failed fatigue specimens have been conducted at NRL.

Experimental Procedure

Two sets of 1/2-in. compact tension (CT) specimens were tested. Each set consisted of two specimens, one cut in the T-L and the other in the L-T orientation.[2] All fatigue tests were conducted in air at room temperature using a constant specimen deformation procedure; the applied load was sinusoidal with a frequency of 13.3 Hz. In this procedure, the value of ΔK increases with crack length even though the applied load is gradually decreased as the length increases. Additional details concerning this testing procedure are given elsewhere [24]. The starting ΔK values used for the two sets of specimens were 22 MPa $\sqrt{m}$ (20 ksi $\sqrt{in.}$) and 16.5 MPa $\sqrt{m}$ (15 ksi $\sqrt{in.}$), respectively. During the cycling the crack length was monitored by a traveling microscope and the ΔK values were computed according to the formula listed in ASTM E-399 [25]. For each test, the log da/dN versus log ΔK curve was obtained by using a seven point incremental polynominal technique as recommended by ASTM E647-78T [26].

At the completion of the fatigue tests, the two sets of specimens were fractured at liquid nitrogen temperature. The fracture surfaces were then examined with a scanning electron microscope (SEM) using an ISI Super-II SEM operated in the high voltage mode. For the purpose of energy dispersive x-ray analysis, the fracture surfaces were also examined with an AMR 1000 SEM equipped with EDAX Model 707B dispersive energy x-ray analyzer.

Results

The FCP data obtained from the specimen tests are presented in Figs. 29 and 30. As shown by both figures, all of the crack growth rates for the first set

[2] The identification convention used is that suggested by ASTM E399 [25].

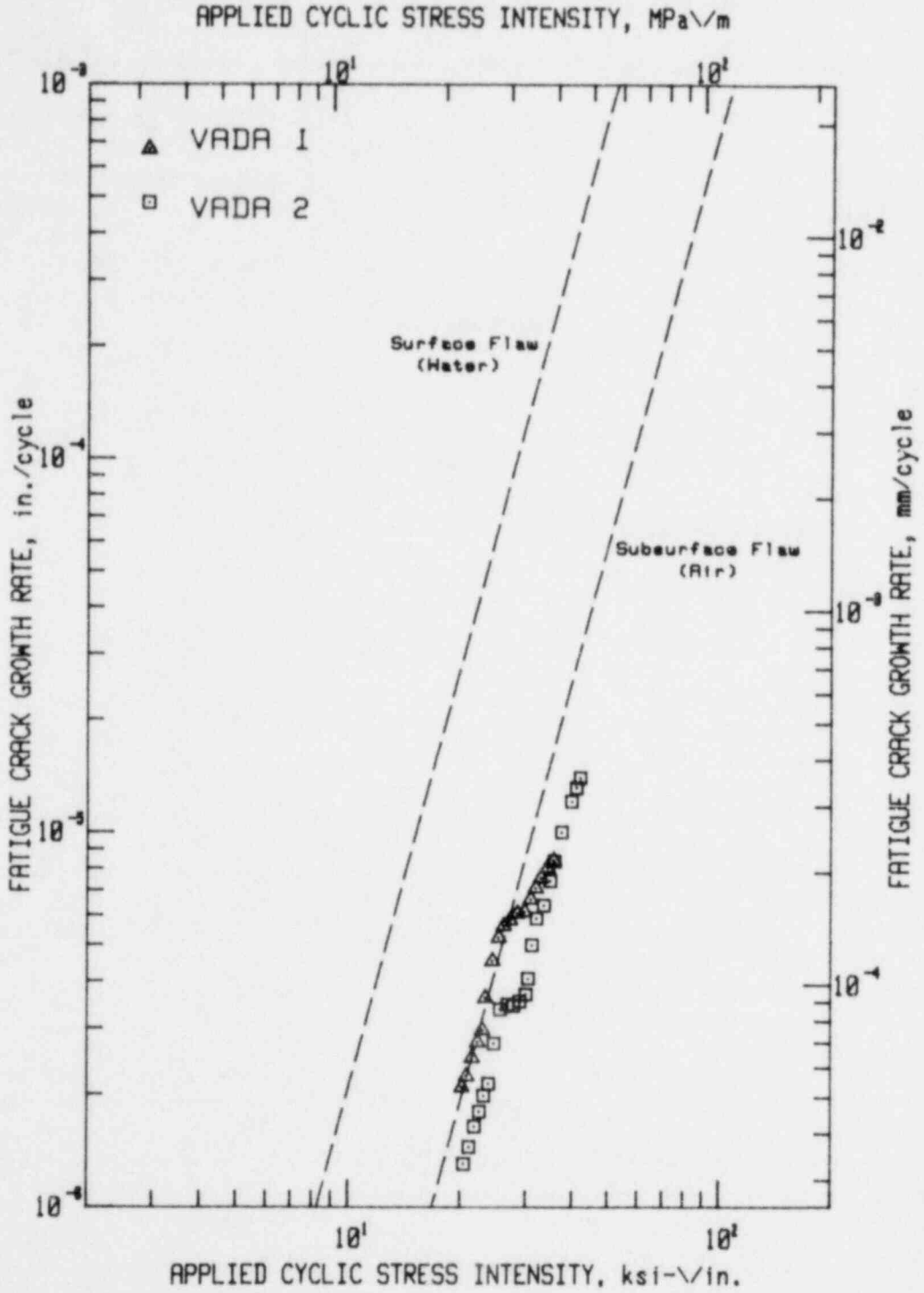

Fig. 29 Fatigue crack propagation data of A302-B ferritic steel tested in air at room temperature both for the T-L (VADA1) and L-T (VADA2) directions with the higher starting ΔK value (22 MPa $\sqrt{m}$).

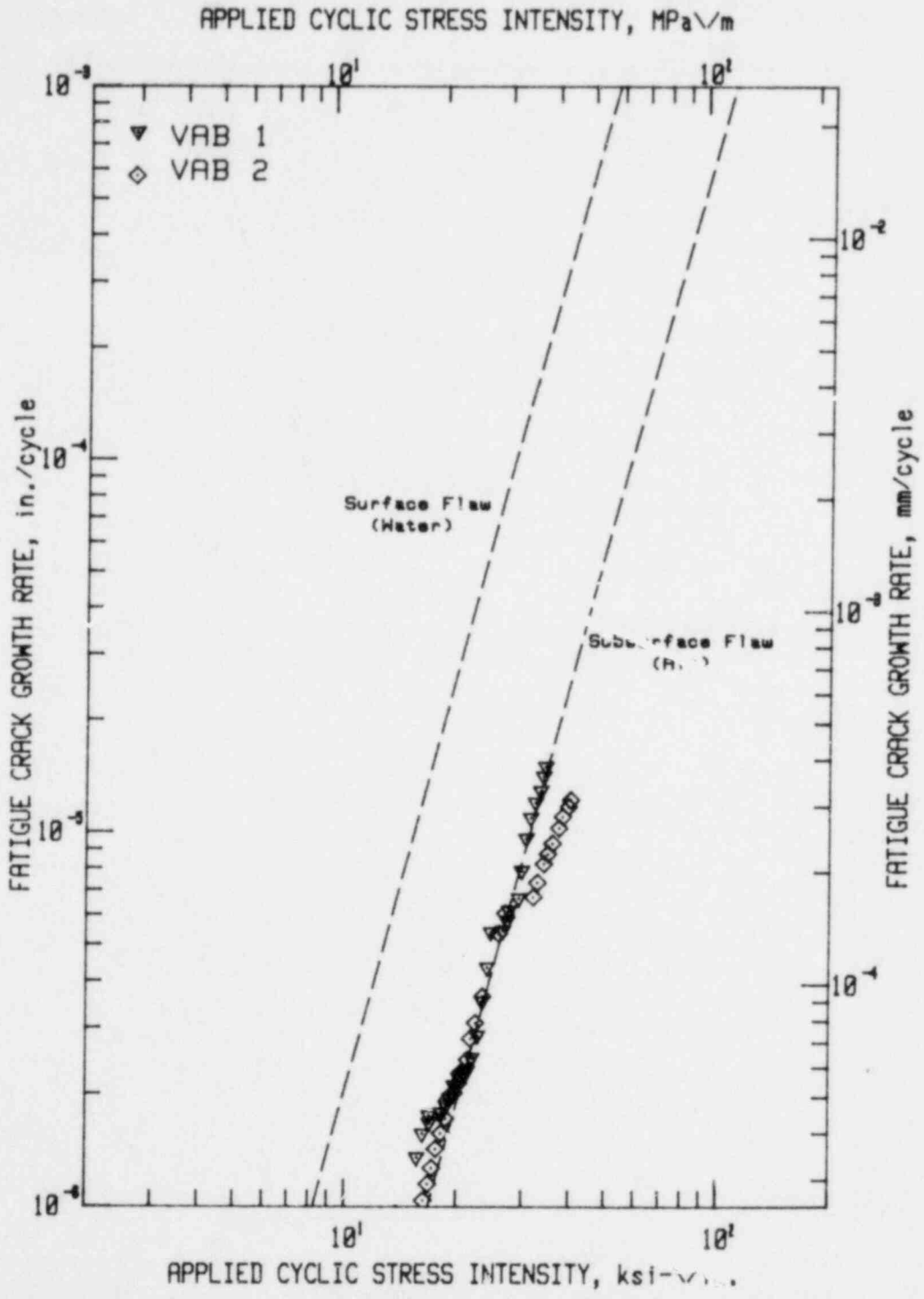

Fig. 30 Fatigue crack propagation data of A302-B ferritic steel tested in air at room temperature both for the T-L (VAB1) and L-T (VAB2) directions with the lower starting ΔK value (16.5 MPa $\sqrt{m}$).

of specimens (Specimen VADA1, cut in the T-L direction, and specimen VADA2, cut in the L-T direction) ran roughly parallel to each other for most of the ΔK range, with the T-L specimen exhibiting the higher crack growth rate (Fig. 29). The crack growth rates for the second set of specimens (specimen VAB1, cut in the T-L direction, and specimen VAB2, cut in the L-T direction) were about equal for ΔK values below 30 MPa $\sqrt{m}$ (27.3 ksi $\sqrt{in.}$). Above this ΔK value, the crack growth rate of the T-L specimen (VAB1) was higher (Fig. 30). The difference in the crack growth behavior in the two sets of specimens are not large. It is interesting to point out, however, that a lower starting ΔK resulted in a higher growth rate (the starting ΔK for VAB1 and VAB2 was 16.5 MPa $\sqrt{m}$, for VADA1 and VADA2, it was 22 MPa $\sqrt{m}$).

The significant fractographic features observed in the SEM examinations of the fracture surfaces are summarized by the micrographs presented in Figs. 31 and 32. In the T-L specimen (VADA1), a microstructural texture running parallel to the macroscopic crack propagation direction is present (Fig. 31). In the second set of tests, the T-L specimen (VAB1) shows an increase in the crack growth rate at ΔK values of 25 to 30 MPa $\sqrt{m}$ (Fig. 30) that coincides with the appearance of the parallel texture in the fracture surface (Fig. 32). Though not shown for the sake of brevity, in the L-T specimen (VAB2), whose corresponding crack growth rate was lower, the parallel texture was absent. The failure mode both for the T-L and L-T specimens was transgranular. In some areas the fracture surfaces were characterized by secondary cracking that ran perpendicular to the macroscopic crack propagation direction. Similar fractographic fractures have been observed in other ferritic steels tested under analogous experimental conditions [27,28].

As observed above, the fracture surface of T-L specimen (VAB1) is characterized by a parallel texture when ΔK exceeds a minimum value in the range of 25 to 30 MPa $\sqrt{m}$. This texture is thought to arise from inclusion bands that are present in the rolled material. To see if the parallel texture is indeed the result of inclusion bands, the fracture surface was analyzed with a x-ray microanalyzer which is attached to AMR 1000 scanning electron microscope. The results of the x-ray microanalysis are summarized in Fig. 33. The analysis confirms that the parallel features were manganese-sulfide inclusion bands.

From the results presented above, it appears that inclusion bands are the primary cause for the increase in the crack growth rate above a minimum ΔK value. It is believed that a preferential decohesion process occurred at the inclusion-matrix interface, which became activated above some threshold stress level and resulted in higher crack growth rates in the specimens cut in the T-L direction. This threshold stress level is probably a measure of the bond strength between the inclusions and the material matrix.

The SEM micrograph shown in Fig. 34 typifies the fractographic features observed in the L-T specimens (VADA2 and VAB2). Together with a small inclusion band, the micrograph reveals the presence of some lamina-shaped holes. These holes are believed to represent the inclusion bands that in the L-T specimens are oriented perpendicular to the main crack path; the few bands that resided along the crack plane did not seem to have affected the crack propagation behavior.

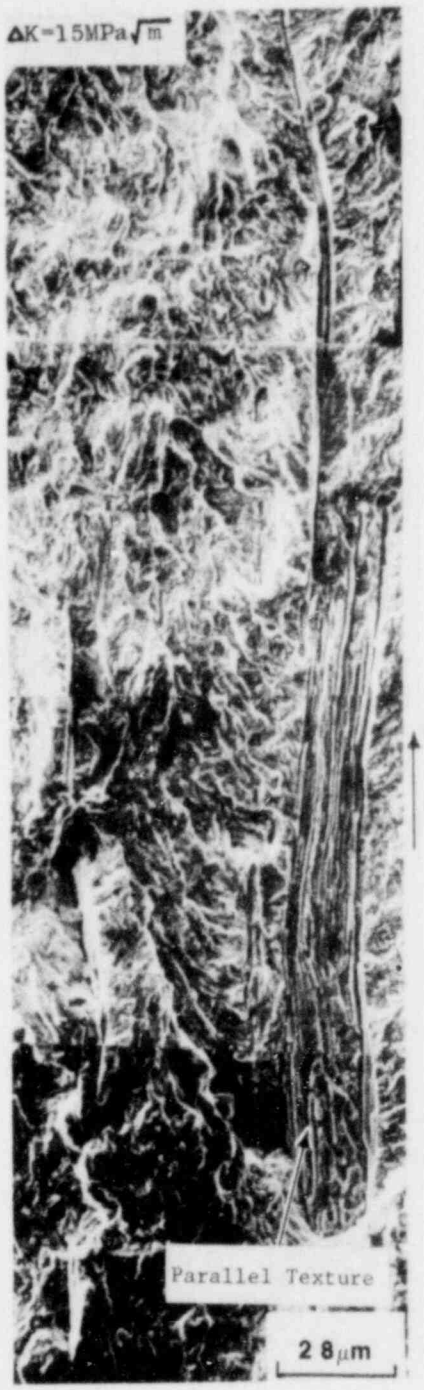

Fig. 31 Fracture surface of A302-B ferritic steel specimen cut along T-L direction (VADAl) tested in air at room temperature with higher starting ΔK value. Arrow shows direction of macroscopic crack propagation. SEM micrographs clearly show inclusion bands in the fracture surface that run parallel to the macroscopic crack propagation direction.

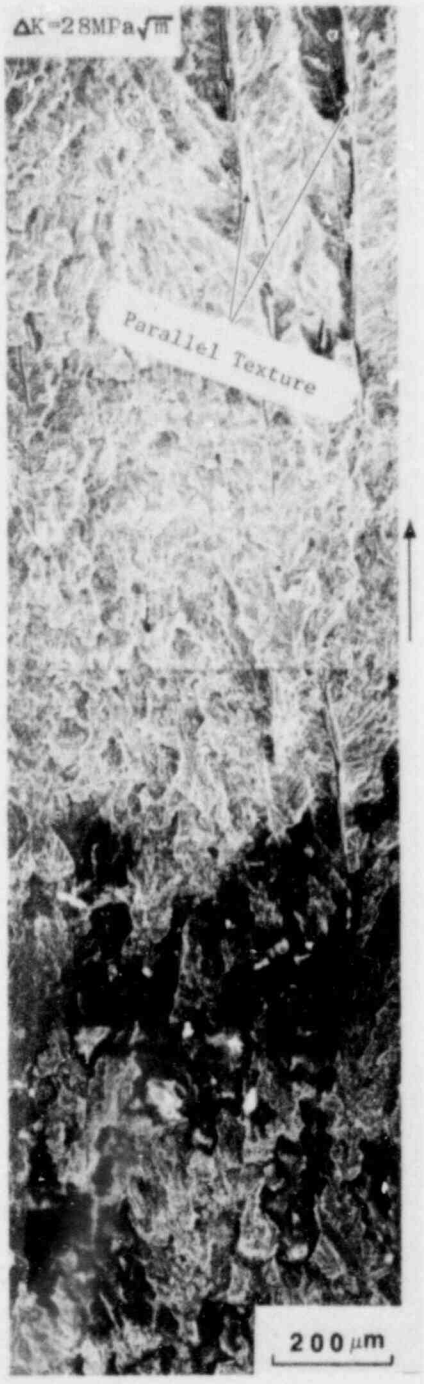

Fig. 32 Fracture surface of A302-B ferritic steel specimen cut along T-L direction (VAB1), tested in air at room temperature with the lower starting ΔK value. Arrow shows direction of macroscopic crack propagation. Series of SEM micrographs show transition region corresponding to 25 to 30 MPa $\sqrt{m}$ ΔK value, where inclusion bands begin to appear in fracture surface.

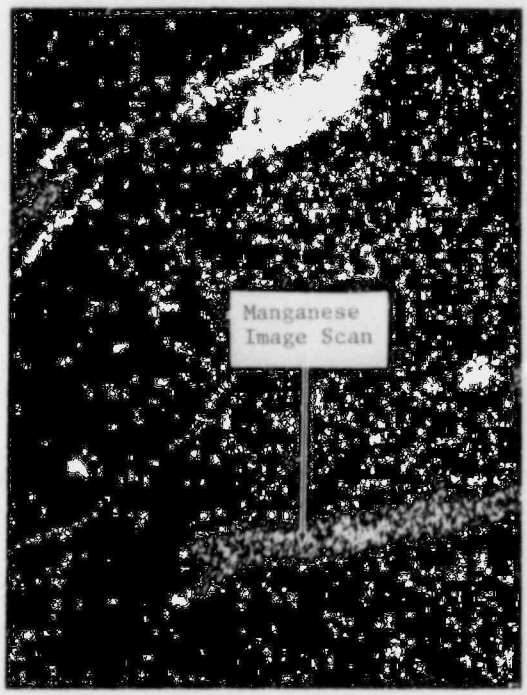

Fig. 33 Fracture surface and corresponding energy dispersive x-ray point maps of A302-B ferritic steel specimen cut along T-L direction (VABl). Arrow shows macroscopic crack propagation direction. SEM micrograph on top of the figure clearly shows inclusion bands in the fracture surface that run parallel to the macroscopic crack propagation direction. Lower two micrographs are image scans obtained through energy dispersive x-ray microanalysis showing that inclusion bands are manganese (left) and sulfur (right) second-phase particles.

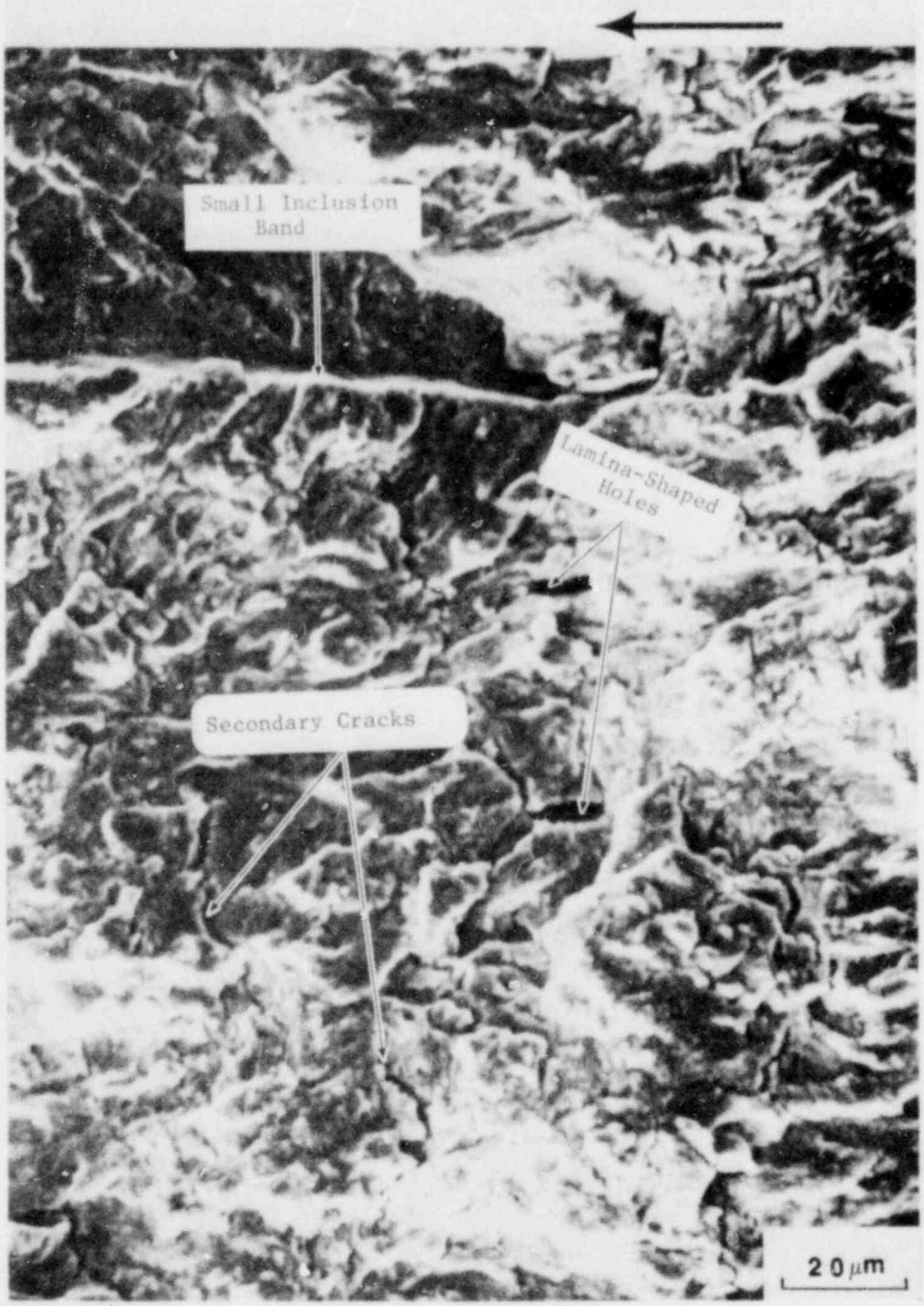

Fig. 34 Fracture surface of A302-B ferritic steel specimen cut along L-T direction (VADA2) tested in air at room temperature. Arrow shows direction of macroscopic crack propagation. SEM micrograph shows small inclusions and lamina-shaped holes present in the fracture surface. The lamina-shaped holes are believed to represent the inclusion bands that are oriented perpendicular to main crack plane.

Summary and Conclusions

The fracture surfaces and the microstructure of A302-B ferritic steel FCP specimens tested at room temperature have been examined by SEM and by energy dispersive x-ray microanalysis. The crack propagation was taken in the T-L and L-T test directions to permit an investigation of the effect of rolling direction on the fatigue crack growth. The results may be summarized as follows:

(1) Inclusion bands in the T-L specimens were strongly aligned in the rolling direction and were observed in the fracture surfaces. The composition of inclusion bands was determined by energy dispersive x-ray analysis; the x-ray microanalysis showed them to be manganese-sulfide inclusions. These bands indicate a preferential decohesion process at the matrix-inclusion interface that resulted in higher crack growth rates in the T-L specimens when compared to the crack growth rates of the L-T specimens.

(2) In the T-L specimen which had been tested with a lower starting ΔK value, inclusion bands were not observed unless ΔK exceeded a minimum value in the range of 25 to 30 MPa $\sqrt{m}$ (22.7 to 27.3 ksi $\sqrt{in.}$). The minimum ΔK value is probably related to the bond strength between the inclusions and the material matrix.

(3) A few small inclusion bands were seen in the fracture surfaces of the L-T specimens. These small inclusions did not appear to have affected the fatigue crack growth behavior of the material cut in the L-T direction. However, some lamina-shaped holes were present and are thought to represent the inclusion bands oriented perpendicular to the crack plane. The presence of few inclusions and the lamina-shaped holes showed, as anticipated, that the inclusion bands in the L-T specimens were mostly oriented perpendicular to the main crack path.

REFERENCES

1. IWG RRPC-78/1, "Coordinated Research Programme on Analyses of the Behaviour of Advanced Reactor Pressure Vessel Steels Under Neutron Irradiation," Vienna, Austria, 17-18 Oct 1977.

2. Hawthorne, J. R., "Radiation Effects Information Generated on the ASTM Reference Correlation-Monitor Steels," ASTM DS 54, American Society for Testing and Materials, Philadelphia, PA, July 1974.

3. "Effect of Residual Elements on Predicted Radiation Damage to Reactor Vessel Materials," Regulatory Guide 1.99, U.S. Nuclear Regulatory Commission, Office of Standards Development, Washington, D.C., Apr. 1977.

4. Loss, F. J., Editor, "Structural Integrity of Water Reactor Pressure Boundary Components, Progress Report ending 31 May 1977," NRL Memorandum Report 3600, Sep.1977

5. Hawthorne, J.R., Watson, H.E., and Loss, F.J., "Exploratory Investigation of Cyclic Irradiation and Annealing Effects on Notch Ductility of A533-B Weld Deposits," ASTM STP 683, American Society for Testing and Materials, Philadelphia, PA, 1979.

6. Hudak, S.J., Jr., Saxena, A., Bucci, R.J., and Malcolm, R.C., "Development of Standard Methods of Testing and Analyzing Fatigue Crack Growth Rate Data - Final Report," AFML TR 78-40, Air Force Materials Laboratory. May 1978.

7. Loss, F.J., Editor, "Structural Integrity of Water Reactor Boundary Components - Progress Report Ending 30 Nov 1977," NRL Memorandum Report 3782, May 1978.

8. Clarke, G.A., and Landes, J.D., "Evaluation of J for the Compact Specimen, "Scientific Paper 78-1D3-JINTF-P1, Westinghouse R&D Center, Pittsburgh, PA, June 12, 1978.

9. Joyce, J.A., Gudas, J.P., "Computer Interactive J_{Ic} Testing of Navy Alloys," ASTM STP 668, American Society for Testing and Materials, April 1977, Philadelphia, PA, pp.451-568.

10. "The Determination of the Elastic-Plastic Toughness Parameter, J_{Ic}," ASTM Committee E24.08.04, ASTM, Philadelphia, PA, Mar 12, 1979.

11. Bamford, W.H., et. al, "Effect of High-Temperature, Primary Reactor Water on the Fatigue Crack Growth of Reactor Vessel Steels," in HSST Quarterly Progress Report for April-June 1977, ORNL/NUREG/TM-147, pp. 16-28, Dec 1977.

12. Bamford, W.H., and Moon, D.M., "Some Mechanistic Observations on the Crack Growth Characteristics of Pressure Vessel and Piping Steels in PWR Environment," Paper #222, Corrosion 79, Atlanta, GA, National Association of Corrosion Engineers, 1979.

13. Bamford, W.H., Moon, D.M., and Ceschini, L.J., "Effect of High-Temperature Primary Reactor Water on the Subcritical Crack Growth of Reactor Vessel Steels" in HSST Quarterly Progress Report for Oct-Dec 1977, ORNL/NUREG/TM-194, pp. 25-35 (May 1978).

14. Bamford, W.H., and Ceschini, L.J., "Effects of High-Temperature Primary Water on the Fatigue Crack Growth of Reactor Vessel Steels" in HSST Quarterly Progress Report for July-Sep. 1977, ORNL/NUREG/TM-166, pp. 38-45, April 1978.

15. Bamford, W.H., Moon, D.M., and Ceschini, L.J., "Effects of High-Temperature Primary Water on the Fatigue Crack Growth of Reactor Vessel Steels" in HSST Quarterly Progress Report for April-June 1978, ORNL/NUREG/TM-239, pp. 9-18, Oct 1978.

16. Bamford, W.H., Moon, D.M., and Ceschini, L.J., "Effects of High-Temperature Primary Water on the Fatigue Crack Growth in Reactor Vessel Steels" in HSST Quarterly Progress Report for July-Sep 1977, ORNL/NUREG/TM-275, pp. 21-29, Jan 1979.

17. Bamford, W. H., Moon, D.M., and Ceschini, L.J., "Effects of High-Temperature Primary Water on the Fatigue Crack Growth of Reactor Vessel Steels" in HSST Quarterly Progress Report for Oct-Dec 1978, ORNL/NUREG/TM-298, pp. 14-23, April 1979.

18. Hale, D.A., Tuen, J., Gerber, T., "Fatigue Crack Growth in Piping and RPV Steels in Simulated BWR Water Environment," GE Report, GEAP-21098, NRC-5, San Jose, CA, Jan 1978.

19. Vosikovsky, O., "Fatigue-Crack Growth in an X-65 Line-Pipe Steel at Low Cyclic Frequencies in Aqueous Environments," Trans. ASME, Ser. H, J. Engineering Mat. and Tech. 97:298-304 (1975).

20. Kondo, T., et. al, "Fatigue Crack Propagation Behaviour of ASTM A533B and A302B Steels in High Temperature Aqueous Environment," Sixth Annual Information Meeting of HSST Program (April 1972).

21. Suzuki, M., et. al, "The Environment Enhanced Crack Growth Effects in Structural Steels for Water Cooled Nuclear Reactors," Paper C125/77 in Proceedings, Institute of Mechanical Engineers, London, pp. 161-169 (1977).

22. Radon, J. C., Branco, C. M., and Culver, L. E., "Crack Blunting and Arrest in Corrosion Fatigue of Mild Steel," Int. J. Fracture 12:467-469 (1976).

23. F. A. Heiser and R. W. Hertzberg, "Anisotropy of Fatigue Crack Propagation, "Trans. ASME, J. Basic Engineering, June 1972, Series D, Vol. 93, pp. 211-217.

24. G. Gabetta, CISE Technical Note (to be published).

25. "Standard Method of Test for Plain-Strain Fracture Toughness of Metallic Materials," ASTM E399-70T, ASTM Standards, Part 10, pp. 512-533, 1978.

26. "Tentative Method of Test for Constant Load-Amplitude Fatigue Crack Growth Rate Above 10^{-8} m/cycle," ASTM E647-78T, ASTM Standards, Part 10, pp. 662-682, 1979.

27. C. E. Richards and T. C. Lindley, Engineering Fracture Mechanics, Vol. 4, pp. 951-958, 1972.

28. W. H. Cullen, et. al, "Fatigue Crack Growth of A508 Steel in High-Temperature, Pressurized Reactor-Grade Water," NRL Memorandum Report (pending publication).

* U. S. GOVERNMENT PRINTING OFFICE : 1979 281-484/113